distances in **4**. Further experimental, as well as theoretical, studies are needed to clarify the reasons for the discrepancy.

Acknowledgment. This work was supported at Utah by the National Cancer Institute of the NIH (2ROCA16903) and at the Technion by the US-Israel Binational Science Foundation (BSF), the Fund for the Promotion of Research, and the S. Faust Research Fund. We thank Professors F. H. Herbstein and M. Kaftory for helpful discussions and G. Berg for the drawings.

Registry No. Propynyl *p*-nitrobenzoate, 113779-41-2; hydroxyacetylene, 32038-79-2; ethynyl formate, 123812-75-9; propynyl formate, 123812-74-8; ethynyl acetate, 83313-98-8; vinyl formate, 692-45-5; methyl formate, 107-31-3.

Hexaazaoctadecahydrocoronene.† Structural and Physical Properties of $[HOC]^n$ (n = 0, 1+, 2+, 3+, 4+)

Joel S. Miller,* David A. Dixon,* Joseph C. Calabrese, Carlos Vazquez, Paul J. Krusic,* Michael D. Ward, E. Wasserman, and Richard L. Harlow

Contribution No. 5098 from the Central Research and Development Department, Experimental Station E328, E. I. du Pont de Nemours & Company, Inc., Wilmington, Delaware 19880-0328.
Received April 10, 1989

Abstract: Hexaazaoctadecahydrocoronene and its mono-, di-, tri-, and tetracations, $[HOC]^n$ (n = 0, 1+, 2+, 3+, 4+), have been prepared and characterized by X-ray diffraction, EPR, magnetic susceptibility, and electronic and vibrational spectroscopies. HOC, $[HOC]^{\bullet+}[BF_4]^-$, $[HOC]^{\bullet+}[TCNE]^{\bullet-}$ (TCNE = tetracyanoethylene), $[HOC]^{\bullet+}[F_3CSO_3]^-$, $[HOC]^{2+}\{[PF_6]^-\}_2$, $[HOC]^{2+}\{[BF_4]^-\}_2$, $[HOC]^{2+}\{[C(CN)_3]^-\}_2$, $[HOC]^{2+}\{C[C(CN)_2]_3\}^{2-}$, $[HOC]^{2+}\{Ni[S_2C_2(CF_3)_2]_2^{\bullet-}\}_2$, $[HOC]^{\bullet3+}\{[PF_6]^-\}_3$, $[HOC]^{\bullet3+}\{[SbF_6]^-\}_3$, and $[HOC]^{4+}\{[SbF_6]^-\}_4$·MeCN have been studied by single-crystal X-ray diffraction. HOC and $[HOC]^{4+}$ have essentially equivalent C_6-ring C–C bond distances averaging 1.397 and 1.436 Å, respectively. Their average C_6-ring C–N distances are 1.416 and 1.318 Å, respectively. The dication, $[HOC]^{2+}$, has a distorted (Jahn–Teller) structure corresponding to coupled cyanine fragments with distinctly different short (1.395-Å) and long (1.471-Å) C_6-ring C–C and C–N (1.337- and 1.405-Å) bond distances. The 1+ and 3+ radical ions also show distorted structures, although the distortions are smaller than observed for the 2+ structure. The short C_6-ring C–C bond distances are 1.382 and 1.417 Å, and the long C_6-ring C–C bond distances are 1.444 and 1.439 Å, while the short C_6-ring C–N bond distances are 1.371 and 1.326 Å and the long C_6-ring C–N bond distances are 1.422 and 1.339 Å, respectively. Solid-state magnetic susceptibility measurements show that the n = 0, 2+, and 4+ compounds are diamagnetic and that the n = 1+ and 3+ salts are $S = {}^1/_2$ paramagnets that obey the Curie–Weiss expression between 2 and 320 K. The effective moments, μ_{eff}, and Curie–Weiss constants, θ, are 1.77 and 1.75 μ_B and θ = −3.3 and −0.9 K for the mono- and trications, respectively. The n = 1+ and 3+ radical cations are fluxional in solution. The EPR spectrum of $[HOC]^{\bullet+}$ in the fast-exchange limit (25 °C) shows that all protons and N's have the same hyperfine splitting (2.56 G, g = 2.003 15). In the slow-exchange limit (−90 °C), there are 2 sets of 12 equivalent protons (0.974 and 4.222 G) and 6 equivalent N's (2.595 G). This precludes the observation of a Jahn–Teller distortion in solution. The $[HOC]^{\bullet3+}$ ion is more fluxional in solution as it exhibits fast-exchange behavior at −60 °C [a(24H) = a(6 N) = 2.81 G; g = 2.0310]. EPR spectra of polycrystalline $[HOC]^{2+}$ salts show the presence of thermally accessible triplet species whose zero-field splitting parameters are $|D|$ = 0.0550 ± 0.0008 cm^{-1} and $|E|$ = 0.0024 ±0.0005 cm^{-1} and are appropriate for triplet states of less than 3-fold symmetry. The temperature dependence of the ΔM = ±2 EPR absorption afforded the separation between the ground singlet state and the excited triplet state of the dication for a variety of $[HOC]^{2+}$ salts. For most counteranions, these separations are greater than 3 kcal/mol (1050 cm^{-1}, 0.13 eV). Solid-state magnetic susceptibility measurements for those $[HOC]^{2+}$ with singlet–triplet gaps less than 4.0 kcal/mol show increases in susceptibilities at higher temperatures, consistent with the presence of thermally populated triplet excited states. Magnetic susceptibility and single-crystal X-ray structures of the dication in the crystalline materials of this study are consistent with a singlet ground state. Molecular orbital (ab initio) calculations are in general agreement with the above results.

With guidance from a model proposed by H. M. McConnell,[1] stable triplet (S = 1) organic species have been deliberately designed[2,3] and synthesized as potential components of s/p-orbital-based molecular ferromagnets.[3,4] This goal has recently been achieved with the characterization of the donor–acceptor complex, DA, $[Fe^{III}(C_5Me_5)_2]^{\bullet+}[TCNE]^{\bullet-}$ as a molecular/organic bulk ferromagnet.[3,5] At the present time, the McConnell model provides a useful conceptual framework for understanding the stabilization of ferromagnetic coupling in this system. The essence of the model is that the energy of the $D^{\bullet+}A^{\bullet-}$ ground state (E_{GS}) is lowered to E'_{GS} by configurational mixing with the $^3D^{:2+}A^{2-}$ excited state[6a] (E_{ES}), thus stabilizing pairwise ferromagnetic coupling, Scheme Ia. Likewise, it is feasible that the energy of a $^3D^{:2+}A^{2-}$ ground state[6b] (E_{gs}) could also be lowered to E'_{gs} by configurational mixing with the $D^{\bullet+}A^{\bullet-}$ excited state (E_{es}) to stabilize ferromagnetic coupling, Scheme Ib. Although triplet $^3[Fe^{III}(C_5Me_5)_2]^{:2+}$ is an unknown species, admixing of the $D^{:2+}A^{2-}$ virtual state with the ground state was invoked to explain the

Scheme I

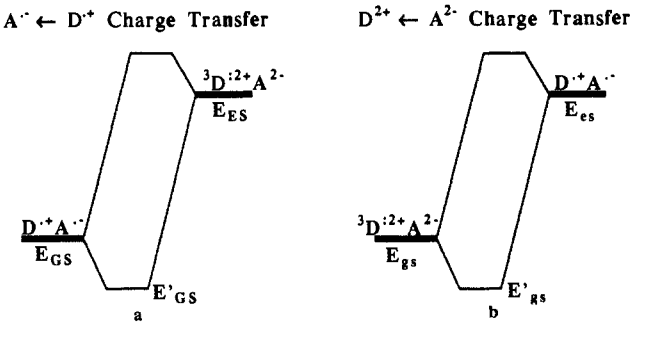

†The ACS Editorial Office suggests dodecahydrohexaazacoronene as a more appropriate name (due to the lower hydrogen content when nitrogen replaces carbon).

(1) McConnell, H. M. *Proc. Robert A. Welch Found. Conf. Chem. Res.* **1967**, *11*, 144.

0002-7863/90/1512-381$02.50/0

ferromagnetic coupling. This indicated that ground-state triplets are not necessary components for a molecular ferromagnet as long as a charge-transfer excited state can virtually admix with the ground state to stabilize ferromagnetic coupling.[2,3,5b] We therefore sought to prepare donor–acceptor electron-transfer salts based on doublet ($S = {}^1/_2$) cations with virtually admixable triplet dications and radical anions previously reported to stabilize ferromagnetic coupling in $[Fe^{III}(C_5Me_5)_2]^{\bullet+}$ salts.[3] Such radical anions include $[TCNQ]^{\bullet-}$ (TCNQ = 7,7,8,8-tetracyano-*p*-quinodimethane), $[TCNE]^{\bullet-}$ (TCNE = tetracyanoethylene), $[DDQ]^{\bullet-}$ (DDQ = 2,3-dichloro-5,6-dicyanobenzoquinone), and $[C_4(CN)_6]^{\bullet-}$.[3a]

Hexaazaoctadecahydrocoronene, HOC, reported by Breslow and co-workers[4c,7a,b,8] in their efforts toward organoferromagnets and by Praefcke and co-workers,[7d] was selected as a model donor for this study[9] since its dication, $[HOC]^{2+}$, had been reported to

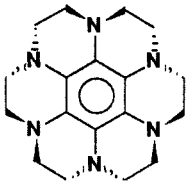

HOC

be a ground-state triplet in certain frozen solutions.[4c,7a,b] The first example of a triplet benzene dication was derived from hexachlorobenzene, which was only stable below 77 K in the highly reactive media in which it was prepared.[10] The presence of an energetically favorable triplet state suggested that virtual admixing of a $^3D^{\cdot2+}A^{2-}$ excited state with a $D^{\bullet+}A^{\bullet-}$ ground state may be significant in providing a mechanism for ferromagnetic interactions. Herein we report the results of our study, which, due to some unexpected observations,[9] was extended to characterize HOC as well as the four oxidation states: monocation, $[HOC]^{\bullet+}$,[7a,b] dication, $[HOC]^{2+}$,[7a,b,9] trication, $[HOC]^{\bullet3+}$, and tetracation, $[HOC]^{4+}$.[8]

Experimental Section

All reactions were performed with standard Schlenk techniques or in an argon-filled recirculating Vacuum Atmospheres Dri-Box using solvents distilled under argon. EPR spectra were recorded either on an IBM/Bruker ER 200 D-SRC or on a Bruker ER 420 spectrometer. Line positions were measured accurately using field markers generated by an NMR gaussmeter while the microwave frequency was measured by a microwave frequency counter. Cyclic voltammetry was performed in acetonitrile solution containing 0.1 M $[n\text{-}Bu_4N][ClO_4]$ electrolyte in a conventional H-cell with a platinum working electrode and a Ag/AgCl reference electrode. Cyclic voltammetry was also measured in liquid SO_2 containing 0.1 M $[n\text{-}Bu_4N][BF_4]$ electrolyte in a single-compartment cell with a platinum counter electrode and a Ag pseudoreference electrode. All potentials are reported versus SCE. Voltammograms were recorded with a Princeton Applied Research 173/175 potentiostat/programmer. Infrared spectra were recorded on a Nicolet 7199 Fourier transform spectrometer; the $\nu_{C\equiv N}$ absorptions are listed in Table I. Electronic absorption spectra in the range 200–1400 nm were acquired on a Cary 2300 spectrophotometer; representative absorption maxima with nonabsorbing anions are presented as supplementary materials.

Magnetic susceptibility measurements were performed with the Faraday method in a Janis Supervariatemp variable-temperature cryostat. The Faraday balance is based on a Cahn 1000 microbalance, Keithley 705 20-channel scanner, Keithley 193 voltmeter, and an Oxford 3120 temperature controller interfaced with a Digital PDP 1173 computer. A Walker magnet with a 25.4-cm (10-in.) pole face was utilized. The conventional $HgCo(SCN)_4$ standard was used to calibrate the apparatus. The samples are suspended on Spectrosil quartz fibers and buckets or KelF buckets. Calibrations of the fibers and buckets were made and used to correct the reported susceptibilities. The typical temperature range is from 2.2 to 320 K with three fields measured between 5.2 and 19.5 kG at each set temperature, although temperatures as low as 1.4 K and fields as low as 200 G can be utilized. Sample weights vary from 1 to 200 mg depending on the magnetic properties of the sample. A special desiccator-based loading technique was devised to load air-sensitive samples without exposing the sample to the atmosphere. The Faraday balance is interfaced with a computer.

TCNE (Aldrich) was sublimed prior to use, and TCNQ (Aldrich) and DDQ (Aldrich) were recrystallized from MeCN and chloroform, respectively, prior to use. $TCNQF_4$,[11a] $C_4(CN)_6$,[11b] $\{[n\text{-}Bu_4N]^+\}_2\{C_3[C(CN)_2]_3\}^{2-}$,[11c] and $[n\text{-}Bu_4N]^+\{C_3[C(CN)_2]_3\}^{\bullet-}$[11c] were prepared via literature routes. 1,3,5-Triamino-2,4,5-trinitrobenzene (Chemtronics) was converted to hexaaminobenzene by a literature route.[12] $Ag[BF_4]$, $Ag[PF_6]$, $Ag[AsF_6]$, $Na[BPh_4]$, $[NO][PF_6]$, $[NO][SbF_6]$, $[NO][AsF_6]$, $[NO][BF_4]$, $K[C(CN)_3]$, and $Ag[CF_3SO_3]$ were used as purchased (Alfa). $Ni[S_2C_2(CF_3)_2]_2$,[11d] $[(Ph_3P)_2N][C(CN)_3]$,[11e] and $[n\text{-}Bu_4N]_2\{C[C(CN)_2]_3\}$[11f] were prepared by literature routes. Elemental analysis was performed by Oneida Research Services, Inc. (Whitesboro, NY), and are typically ±0.3% of the calculated values, Table I. Mass spectra were obtained on a VG Micromass 7070HS mass spectrometer using 70-eV electrons as the ionization source.

Hexaazaoctadecahydrocornene [HOC]. HOC was prepared from 2a,4a,6a,8a,10a,12a-hexaazacoronene-1,3,5,7,9,11(2*H*,4*H*,6*H*,8*H*,10*H*,12*H*)-hexone following a brief report.[7a] The hexaketone (2.30 g, 5.6 mmol) was placed in a flame-dried 300-mL round-bottom flask. Borane/THF (Aldrich; 75 mL, 1.0 M) was added via syringe under nitrogen. The slurry was then heated under reflux for 16 h prior to cooling to ice temperature. To the cooled slurry, 75 mL of degassed 6 N HCl was slowly added, after which the solvent was pumped off and another 75 mL of degassed 6 N HCl was added to the residue. This mixture was filtered under nitrogen, and the filtrate was neutralized with 6 N degassed NaOH. A white solid precipitate formed and was collected via vacuum filtration under nitrogen. After washing with 2 × 50 mL degassed water, the product was dried under nitrogen overnight and stored at −30 °C in a glovebox (yield: 1.42 g, 4.38 mmol; 78%). The product was recrystallized from a minimum amount of dichloromethane, and crystals suitable for X-ray studies were prepared by slow diffusion of diethyl ether into a dichloromethane solution of the product. The high-resolution mass spectrum shows *m/e* at 324.2064 (324.2062 calcd) P^+, 295.1659 (295.1671) $P - C_2H_5^+$, 281.1514 (281.1514) $P - C_3H_8^+$, and 162.1053 (162.1031) $P - C_9H_{12}N_3^+$. Electronic absorption spectrum (CH_2Cl_2): 260 nm (17 600 M^{-1} cm^{-1}).

Hexaazaoctadecahydrocoronenium Tetraphenylborate, $[HOC]^{\bullet+}[BPh_4]^-$. A solution containing 80 mg of HOC (0.247 mmol) dissolved in 10 mL of CH_2Cl_2 was added to 5 mL of MeCN containing 103 mg (0.247 mmol) of $Ag[BPh_4]$ {prepared from $Ag[NO_3]$ and $Na[BPh_4]$}. The silver precipitate was filtered off and crystals of the product formed upon diethyl ether diffusion into the filtrate over a period of 4 days. The product was collected by vacuum filtration; yield 148 mg, 93%. A crystal

(2) Miller, J. S.; Epstein, A. J. *J. Am. Chem. Soc.* **1987**, *109*, 3850.
(3) (a) Miller, J. S.; Epstein, A. J.; Reiff, W. M. *Chem. Rev.* **1988**, *88*, 201–220. (b) Miller, J. S.; Epstein, A. J. *NATO Adv. Study Inst. Ser., Ser. B* **1988**, *168*, 159–174. (c) Miller, J. S.; Epstein, A. J.; Reiff, W. M. *Acc. Chem. Res.* **1988**, *21*, 114–120. (d) Miller, J. S.; Epstein, A. J.; Reiff, W. M. *Science* **1988**, *240*, 40–47.
(4) (a) Breslow, R. *Pure Appl. Chem.* **1982**, *54*, 927. (b) Breslow, R.; Jaun, R.; Klutz, Q.; Xia, C.-Z. *Tetrahedron* **1982**, *38*, 863. (c) Breslow, R. *Mol. Cryst. Liq. Cryst.* **1985**, *125*, 261.
(5) (a) Miller, J. S.; Calabrese, J. C.; Bigelow, R. W.; Epstein, A. J.; Zhang, J. H.; Reiff, W. M. *J. Chem. Soc., Chem. Commun.* **1986**, 1026. (b) Miller, J. S.; Calabrese, J. C.; Rommelmann, H.; Chittapeddi, S.; Zhang, J. H.; Reiff, W. M.; Epstein, A. J. *J. Am. Chem. Soc.* **1987**, *109*, 769. (c) Chittapeddi, S.; Kromack, S.; Miller, J. S.; Epstein, A. J. *Phys. Rev. Lett.* **1987**, *58*, 2695–2698.
(6) (a) Alternatively with the acceptor being the triplet $D^{2+}A^{\cdot2-}$. (b) A system for this is $[HOC]^{2+}\{C_3[C(CN)_2]_3\}^{2-}$.[4c]
(7) (a) Breslow, R.; Maslak, P.; Thomaides, J. S. *J. Am. Chem. Soc.* **1984**, *106*, 6453. (b) Thomaides, J. S.; Maslak, P.; Breslow, R. *J. Am. Chem. Soc.* **1988**, *110*, 3970–3979. (c) LePage, T. J.; Breslow, R. *J. Am. Chem. Soc.* **1987**, *109*, 6412. (d) Kohne, B.; Praefcke, K.; Reichmann, A. *Chem.—Ztg.* **1985**, *109*, 17.
(8) Dixon, D. A.; Calabrese, J. C.; Harlow, R. L.; Miller, J. S. *Angew. Chem., Int. Ed. Engl.* **1989**, *28*, 92.
(9) Miller, J. S.; Dixon, D. A.; Calabrese, J. C. *Science* **1988**, *240*, 1185–1188.
(10) Wasserman, E.; Hutton, R. S.; Kuck, V. J.; Chandross, E. A. *J. Am. Chem. Soc.* **1974**, *95*, 1965. More than 20 benzene derivatives with 3-fold or higher symmetry were examined under the strong oxidizing conditions used in the hexachlorobenzene study. Except for the possible formation of a triplet in the 1,3,5-trichloro-2,4,6-trifluorobenzene dication, no triplets were observed (Wasserman, E., private communication).
(11) (a) Wheland, R. C.; Martin, E. L. *J. Org. Chem.* **1975**, *40*, 1301. (b) Webster, O. *J. Am. Chem. Soc.* **1964**, *86*, 2898–2902. (c) Fukunaga, T. *J. Am. Chem. Soc.* **1976**, *98*, 610. Fukanaga, T. *J. Am. Chem. Soc.* **1976**, *98*, 611. U.S. Patent US 3,963,769, 1976. (d) Davision, A.; Holm, R. H. *Inorg. Synth.* **1967**, *10*, 8–26. McCleverty, J. A. *Prog. Inorg. Chem.* **1968**, *10*, 49–222. (e) Dixon, D. A.; Calabrese, J. C.; Miller, J. S. *J. Am. Chem. Soc.* **1986**, *108*, 2582. (f) Middleton, W. J.; Little, E. L.; Coffman, D. D.; Englehard, V. A. *J. Am. Chem. Soc.* **1958**, *80*, 2795.
(12) Rogers, D. Z. *J. Org. Chem.* **1986**, *51*, 3905–3907.

Table I. Summary of Elemental Analysis and Infrared Data for $[HOC]^{n}$ (n = 1+,2+,3+,4+)

anion, A	HOC/A	%C		%H		%N		$\nu_{C\equiv N}$
		calcd	obsd	calcd	obsd	calcd	obsd	
$[BF_4]^-$	1:1	52.57	52.06	5.88	5.65	20.44	20.37	
$[BF_4]^-$	1:2	43.41	43.23	4.86	4.75	16.87	16.85	
$[PF_6]^-$	1:1	46.06	45.98	5.15	4.89	17.90	17.81	
$[PF_6]^-$	1:2	35.19	35.04	3.94	3.74	13.68	13.52	
$[PF_6]^-$	1:3	28.47	28.44	3.19	2.99	11.07	10.95	
$[AsF_6]^-$	1:1	42.11	41.44	4.72	4.46	16.37	15.97	
$[AsF_6]^-$	1:2	30.79	30.65	3.44	3.39	11.97	11.93	
$[SbF_6]^-$	1:1	38.59	38.39	4.33	4.21	15.01	14.86	
$[SbF_6]^-$	1:2	27.57	27.61	3.09	2.69	10.72	10.28	
$[SbF_6]^{\bullet-}$	1:3	20.96	20.91	2.34	2.96	8.15	7.97	
$[SbF_6]^-$	2:7	18.81	18.86	2.10	2.11	7.31	7.52	
$[SbF_6]^-$	2:7	18.81	18.55	2.10	1.92	7.31	7.31	
$[SbF_6]^{\bullet-}$	1:4	17.06	16.69	1.91	1.85	6.63	6.56	
$[SbF_6]^{\bullet-}$·MeCN	1:4	17.60	17.91	2.10	1.86	7.56	7.16	
$[BPh_4]^-$	1:1	78.37	77.52	6.86	6.94	13.06	13.17	
$[CF_3SO_3]^-$	1:1	46.61	47.76	4.94	4.94	17.16	17.55	
$[CF_3SO_3]^-$	1:2	38.59	38.54	3.89	3.80	13.50	13.27	
$[C(CN)_3]^-$	1:2	61.89	61.66	4.79	4.54	33.31	33.23	2154 s, 2162 m
$[TCNE]^{\bullet-}$	1:1	63.70	63.10	5.35	5.06	30.95	30.56	2145, 2184
$[TCNE]^{\bullet-}$	1:2	62.06	62.59	4.17	3.98	33.77	33.98	2159 s, 2175 s, 2190 m
$[TCNQ]^{\bullet-}$	1:1	68.16	68.36	5.34	5.05	26.50	26.39	2121 m, 2163 m
$[TCNQF_4]^{\bullet-}$	1:1	60.00	59.81	4.03	3.97	23.32	23.27	2090, 2140, 2168
$[i\text{-}C_4(CN)_6]^{\bullet-}$	1:1	63.63	63.15	4.58	4.24	31.80	31.70	2166 m, 2177 s
$[n\text{-}C_4(CN)_6]^{\bullet-}$	1:1	63.63	63.20	4.58	4.27	31.80	31.43	2127, 2166
$\{C_3[C(CN)_2]_3\}^{\bullet-}$	1:1	65.21	64.96	4.38	4.05	30.42	29.98	2167 m, 2185 s
$\{C_3[C(CN)_2]_3\}^{\bullet-}$	1:2	64.61	64.52	3.10	3.02	32.29	31.71	2166 s, 2184 s, 2210 m
$[DDQ]^{\bullet-}$·MeCN	1:1	56.77	56.61	4.59	4.38	21.28	21.09	2216
$\{Ni[S_2C_4F_6]_2\}^{\bullet-}$	1:2	30.34	30.40	1.80	1.54	6.24	6.16	

belonging to the monoclinic space group $C2/c$ was isolated [a = 25.589 (6) Å, b = 13.477 (3) Å, c = 16.072 (4) Å, β = 112.10 (2)°, Z = 4, and V = 5135 Å^3]. Due to the large weighted R_w factor of 0.131 arising from disorder, this structure is not reported.

Hexaazaoctadecahydrocoronenium tetrafluoroborate ($[HOC]^{\bullet+}[BF_4]^-$), **hexafluorophosphate** ($[HOC]^{\bullet+}[PF_6^-]$), **hexafluoroantimonate** ($[HOC]^{\bullet+}[SbF_6]^-$), **hexafluoroarsenate** ($[HOC]^{\bullet+}[AsF_6]^-$), **triflate** ($[HOC]^{\bullet+}[F_3CSO_3]^-$), **tetracyanoethylenide** ($[HOC]^{\bullet+}[TCNE]^{\bullet-}$), **7,7,8,8-tetracyano-*p*-benzoquinonedimethanide** ($[HOC]^{\bullet+}[TCNQ]^{\bullet-}$), **hexacyanobutadienediide** ($[HOC]^{2+}[n\text{-}C_4(CN)_6]^{2-}$), **2,3-dichloro-5,6-dicyanobenzoquinonide** ($[HOC]^{\bullet+}[DDQ]^{\bullet-}$), **and perfluoro-7,7,8,8-tetracyano-*p*-benzoquinonedimethanediide** ($[HOC]^{2+}[TCNQF_4]^{2-}$) were prepared via the above methodology.

Hexaazaoctadecahydrocoronenium hexacyanotrimethylenecyclopropanediide, $[HOC]^{2+}\{C_3[C(CN)_2]_3\}^{2-}$, was prepared via reaction of $[HOC][SbF_6]_2$ (57 mg, 0.072 mmol) dissolved in 10 mL of MeCN and $[n\text{-}Bu_4N]_2\{C_3[C(CN)_2]_3\}$ (51 mg, 0.072 mmol) dissolved in 25 mL of MeCN. Of the dark red-orange 1:1 product, 39 mg (98%) quickly precipitated and was isolated by vacuum filtration.

Hexaazaoctadecahydrocoronenium bis(tetracyanoethylenide) ($[HOC]^{2+}\{[TCNE]^-\}_2$), **bis(tetrafluoroborate)** ($[HOC]^{2+}\{[BF_4]^-\}_2$), **bis(hexafluorophosphate)** ($[HOC]^{2+}\{[PF_6]^-\}_2$), **bis(hexafluoroarsenate)** ($[HOC]^{2+}\{[AsF_6]^-\}_2$), **ditriflate** ($[HOC]^{2+}\{[F_3CSO_3]^-\}_2$), **bis(hexafluoroantimonate)** ($[HOC]^{2+}\{[SbF_6]^-\}_2$), **and bis(perfluoromethyldithiolato)nickelate** ($[HOC]^{2+}\{Ni[S_2C_2(CF_3)_2]_2^{\bullet-}\}_2$) were prepared via the above methodology using 2 equiv of the oxidant. The monoclinic unit cell of $[HOC]^{2+}\{[F_3CSO_3]^-\}_2$ was determined to be a = 7.105 (4) Å, b = 19.018 (4) Å, c = 9.243 (2) Å, α = 90.00 (2)°, β = 99.96 (3)°, γ = 90.00 (3)°, and V = 1230 Å^3. The structure was determined to be disordered and thus was not refined. The structure of $[HOC]^{2+}\{[BF_4]^-\}_2$ was determined, vide infra. A second, $P2_1/n$ monoclinic polymorph [a = 5.559 (2) Å, b = 19.093 (5) Å, c = 9.768 (4) Å, β = 102.22 (3)°, and V = 1013 Å^3] was identified. Solution of this phase was thwarted due to disorder and is not reported. The monoclinic $P2_1/n$ unit cell of $[HOC]^{2+}\{[SbF_6]^-\}_2$ was determined to be a = 7.429 (1) Å, b = 19.474 (2) Å, c = 9.029 (2) Å, β = 107.43 (1)°, and V = 1246.3 Å^3. Due to disorder of a bridging CH_2CH_2 group, the structure is of relatively poor quality and is not discussed.

Hexaazaoctadecahydrocoronenium bis(tricyanomethanide), $[HOC]^{2+}\{[C(CN)_3]^-\}_2$, was prepared from $[HOC]^{2+}\{[CF_3SO_3]^-\}_2$ (74 mg, 0.119 mmol) and $[(Ph_3P)_2N]^+[C(CN)_3]^-$[11e] (150 mg, 0.24 mmol) in acetonitrile. Diffusion of diethyl ether afforded shiny dark crystals (73%) which were isolated by vacuum filtration.

Hexaazaoctadecahydrocoronenium bis(hexacyanotrimethylenecyclopropanide), $[HOC]^{2+}\{C_3[C(CN)_2]_3^{\bullet-}\}_2$, was prepared via reaction of $[HOC]^{2+}\{[SbF_6]^-\}_2$ (60 mg, 0.075 mmol) dissolved in 5 mL of MeCN and $[n\text{-}Bu_4N]_2\{C_3[C(CN)_2]_3\}$[11c] (71 mg, 0.15 mmol) dissolved in 5 mL of MeCN. A quickly formed precipitate was redissolved by warming the solution, and upon slow diffusion of diethyl ether a purple crystalline product formed (43 mg, 67%), which was isolated by vacuum filtration.

Hexaazaoctadecahydrocoronenium hexacyanoisobutadienediide, $[HOC]^{2+}\{C[C(CN)_2]_3\}^{2-}$, was prepared from HOC by the above procedure using $[n\text{-}Bu_4N]_2[C[C(CN)_2]_3]$.[11f]

Hexaazaoctadecahydrocoronenium tris(hexafluorophosphate) ($[HOC]^{\bullet3+}\{[PF_6]^-\}_3$) **and tris(hexafluoroantimonate)** ($[HOC]^{\bullet3+}\{[SbF_6]^-\}_3$) were prepared by the methodology described for the $[BPh_4]^-$ salt using 3 equiv of the appropriate $[NO]^+$ oxidant.

Hexaazaoctadecahydrocoronenium tetrakis(hexafluoroantimonate), $[HOC]^{4+}\{[SbF_6]^-\}_4$·MeCN, was prepared by the above methodology using 4 equiv of $[NO]^+[SbF_6]^-$. Sometimes homogeneous mixtures of $[HOC]^{\bullet3+}$ and $[HOC]^{4+}$ were obtained. Elemental analyses characterizing the materials as the salts $[HOC][SbF_6]_x$ ($x \sim 3.5$) are reported in Table I.

Theory. Ab initio molecular orbital calculations on $[HOC]^{n}$ (n = 0, 1+, 2+, 3+, 4+) were performed with the STO-3G[13] minimal basis set (144 orbitals). All calculations were done with the GRADSCF[14] and GAMESS[15] programs on a CRAY X-MP/24 supercomputer. Calculations on singlet HOC, $[HOC]^{2+}$, and $[HOC]^{4+}$ were done within the RHF formalism, whereas calculations on $[HOC]^{+}$ (doublet), $[HOC]^{2+}$ (triplet), and $[HOC]^{3+}$ (doublet) were done within the UHF formalism. The geometries were gradient optimized.[16] The gradient optimization of the $[HOC]^{2+}$ triplets was complicated by slow convergence in the UHF/SCF calculations. A similar problem was noted for the doublet $[HOC]^{\bullet3+}$. Force fields were calculated analytically for the singlet states,[17] and MP-2

(13) Hehre, W. J.; Stewart, R. F.; Pople, J. A. *J. Chem. Phys.* **1969**, *51*, 2657.

(14) GRADSCF is an ab initio gradient program system designed and written by A. Komornicki at Polyatomics Research, Mountain View, CA.

(15) GAMESS program system from M. Schmidt, North Dakota State University and S. Elbert, Iowa State University based on the original program from NRCC by: Dupuis, M.; Spangler, D.; Wendoloski, J. J. *National Resource for Computation in Chemistry Software Catalog*; Lawrence Berkeley Laboratory, USDOE: Berkeley, CA, 1980, Program QG01. See also Dupuis, M.; Rys, J.; King, H. F. *J. Chem. Phys.* **1976**, *65*, 111.

(16) (a) Pulay, P. In *Applications of Electronic Structure Theory*; Schaefer, H. F., III, Ed.; Plenum: New York, 1977; Chapter 4. (b) Komornicki, A.; Ishida, K.; Morokuma, K.; Ditchfield, R.; Conrad, M. *Chem. Phys. Lett.* **1977**, *45*, 595.

(17) (a) King, H. F.; Komornicki, A. *J. Chem. Phys.* **1986**, *84*, 5645. (b) King, H. F.; Komornicki, A. In *Geometrical Derivatives of Energy Surfaces and Molecular Properties*; Jorgenson, P., Simons, J., Eds.; NATO ASI Series C; D. Reidel: Dordrecht, 1986; Vol. 166, p 207.

correlation energy calculations were also done on the singlets.[18] The optimized molecular coordinates are given as supplementary material.

X-ray Structure Determination. X-ray Data Collection. Crystals of HOC, $[HOC][BF_4]$, $[HOC][F_3CSO_3]$, $[HOC][TCNE]$, $[HOC][BF_4]_2$, $[HOC][PF_6]_2$, $[HOC][C(CN)_3]_2$, $[HOC]\{C[C(CN)_2]_3\}$, $[HOC]\{Ni[S_2C_2(CF_3)_2]_2\}_2$, $[HOC][PF_6]_3$, $[HOC][SbF_6]_3$, and $[HOC][SbF_6]_4\cdot MeCN$ were grown by diethyl ether or dichloromethane diffusion into acetonitrile solutions of the $[HOC]^{n+}$ salts. Cell constants and an orientation matrix for the data collection were obtained by the usual method from approximately 25 reflections. Systematic absences and subsequent least-squares refinement determined the space groups. During data collection, the intensities of several representative reflections were measured as a check on crystal stability. Where there was a loss of intensity during data collection, an isotropic decay correction (<3%), was applied. Equivalent reflections were merged, and only those for which $(F_o)^2 > 3\sigma(F_o)^2$ were included in the refinement, where $\sigma(F_o)^2$ is the standard deviation based on counting statistics. Data were also corrected for Lorentz and polarization factors. Crystallographic details are summarized in Table II.

Structure Solution and Refinement. The structures of HOC, $[HOC][BF_4]$, $[HOC][TCNE]$, $[HOC][F_3CSO_3]$, $[HOC][C(CN)_3]_2$, $[HOC]\{C[C(CN)_2]_3\}$, $[HOC][SbF_6]_3$, and $[HOC][BF_4]_2$ were solved by direct methods, while $[HOC][PF_6]_2$, $[HOC]\{Ni[S_2C_2(CF_3)_2]_2\}_2$, $[HOC][PF_6]_3$, and $[HOC][SbF_6]_4\cdot MeCN$ were solved by automated Patterson analysis. For HOC, $[HOC][F_3CSO_3]$, $[HOC][BF_4]_2$, $[HOC][PF_6]_2$, $[HOC][C(CN)_3]_2$, $[HOC]\{Ni[S_2C_2(CF_3)_2]_2\}_2$, and $[HOC][TCNE]$, the asymmetric unit contains one-half of the molecules that are related by an inversion center. The $[HOC][BF_4]$, $[HOC][PF_6]_3$, and $[HOC][SbF_6]_4$ salts possess $2/m$ crystallographic symmetry. In contrast, $[HOC]\{C[C(CN)_2]_3\}$ has no crystallographic symmetry. For $[HOC][BF_4]_2$, $[HOC][PF_6]_2$, $[HOC][]C(CN)_3]_2$, and $[HOC][SbF_6]_4\cdot MeCN$, the hydrogen atoms were refined. For the remaining structures, the hydrogen atoms were placed at calculated positions [$(r(C-H) = 0.95$ Å)]. All structures were refined by full-matrix least squares of $\sum w[|F_o| - |F_c|]^{1/2}$ with the neutral atom scattering factors taken from the literature. Except for the bond distances, Table III, most of the crystal structure data are given in the supplementary material.

Nuclear Magnetic Resonance. NMR spectra are not informative for the compounds of this study. The 1+ and 3+ salts are paramagnetic and do not give narrow-line NMR spectra. HOC reacts with impurities and/or residual oxygen in CH_2Cl_2, forming traces of $[HOC]^{\bullet+}$ (detectable by EPR) resulting in contact-shifted broad ^1H and ^{13}C NMR spectra. We have not been able to obtain the narrow-line NMR spectra anticipated for $[HOC]^0$. Broadened NMR spectra were also observed for $[HOC]^{4+}$. This is presumably due to trace amounts of $[HOC]^{\bullet 3+}$.

In contrast to our preliminary report[10] of sharp-line NMR spectra for $[HOC]^{2+}$, subsequent attempts to obtain ^{13}C or ^1H NMR spectra of $[HOC]^{2+}$ were unsuccessful, and the reported spectra were attributed to impurities. This is undoubtedly due to the presence of thermally populated $^3[HOC]^{2+}$ triplets (vide infra) and exchange broadening. Attempts to obtain ^{13}C and ^1H NMR spectra on solid samples were also unsuccessful. For $[HOC][C(CN)_3]_2$ and $[HOC][CF_3SO_3]_2$, only the anions were discernible by ^{13}C NMR: $[C(CN)_3]^-$ at 5.9, $[C(CN)_3]^-$ at 121.8, and $[CF_3SO_3]^-$ at 118.3 ppm.

Results and Discussion

Chemistry. Hexaazaoctadecahydrocoronene is a colorless, extraordinarily air-sensitive solid. Cyclic voltammetry revealed four reversible one-electron oxidation processes at −0.44, +0.06, +0.52, and +0.92 V versus SCE (MeCN) for the 0/+, +/2+, 2+/3+, and 3+/4+ redox couples, respectively, Figure 1.[19] These values agree with those in ref 7b but not with those originally reported in ref 7a. Cyclic voltammetry of $[HOC]^{\bullet+}$ in SO_2 (l)/0.1 M $[n\text{-}Bu_4N]^+[BF_4]^-$ at −40 °C also revealed reversible waves for these events at −0.29, 0.17, 0.53, and 1.02 V versus a Ag pseudoreference electrode. Additionally, a slightly irreversible one-electron wave attributed to the 4+/5+ couple was observed at 2.60 V {$E°(4+/5+) = 2.50$ V versus SCE by comparison with the 3+/4+ value obtained in MeCN}.

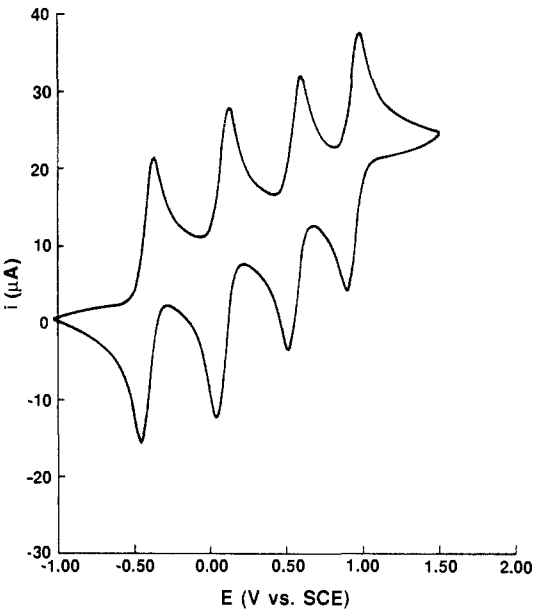

Figure 1. Cyclic voltammetry of HOC in 0.1 M $[n\text{-}Bu_4N][ClO_4]$ in MeCN; V versus SCE.

The electrochemical properties indicated that the preparation of $[HOC]^n$ (n = 1+, 2+, 3+, 4+) cations could be realized by oxidation with Ag^+ or $[NO]^+$. Accordingly, the 1:1 salts of $[BPh_4]^-$, $[CF_3SO_3]^-$, $[BF_4]^-$, $[AsF_6]^-$, $[SbF_6]^-$, and $[PF_6]^-$ and the 1:2 salts of $[BF_4]^-$, $[AsF_6]^-$, $[SbF_6]^-$, $[CF_3SO_3]^-$, and $[PF_6]^-$ were prepared and isolated as crystalline solids, Table I. The redox potentials of the $[HOC]^{n+}/[HOC]^{(n+1)+}$ couples also indicated that oxidation with strong polycyano acceptors was feasible. Addition of equimolar amounts of either TCNE or TCNQ led to the formation of the monocation as either $[HOC]^{\bullet+}[TCNE]^{\bullet-}$ or $[HOC]^{\bullet+}[TCNQ]^{\bullet-}$. Stronger electron acceptors, e.g., $C_4(CN)_6$ and $TCNQF_4$, form 1:1 $[HOC]^{2+}[A]^{2-}$ salts as evidenced by the strong $\nu_{C\equiv N}$ infrared absorptions at 2127 and 2151 cm^{-1} and 2139 and 2166 cm^{-1}, respectively, comparable to values previously reported for the dianions.[20] $[HOC]^{2+}$ salts with two polycyano monoanions, e.g., $[HOC]^{2+}\{[TCNE]^-\}_2$ or $[HOC]^{2+}\{[TCNQ]^-\}_2$, can also be formed with excess acceptor.

In an attempt to induce the dication to crystallize with at least C_3 symmetry, diamagnetic anions with 3-fold axes, i.e., D_{3h} $[C(CN)_3]^-$ and $\{C_3[C(CN)_2]_3\}^{2-}$ or C_{3v} $\{C[C(CN)_2]_3\}^{2-}$, were investigated. Since neutral forms of these anions are unknown, syntheses of these salts were accomplished by metathesis reactions of $[n\text{-}Bu_4N]_2\{C[C(CN)_2]_3\}$, $[(Ph_3P)_2N][C(CN)_3]$, and $[n\text{-}Bu_4N]_2\{C_3[C(CN)_2]_3\}$ with $[HOC][F_3CSO_3]_2$ or $[HOC][AsF_6]_2$. Since for $[HOC]\{C_3[C(CN)_2]_3\}$ the $\nu_{C\equiv N}$ absorptions of 2167 and 2185 cm^{-1} agree well with values previously reported for $\{C_3[C(CN)_2]_3\}^{2-}$;[11c,20] this salt is best formulated as $[HOC]^{2+}\{C_3[C(CN)_2]_3\}^{2-}$. The same salt is obtained using 2 equiv of $[n\text{-}Bu_4N]^+\{C_3[C(CN)_2]_3\}^{\bullet-}$. Likewise $[HOC]^{2+}\{C[C(CN)_2]_3\}^{2-}$ ($\nu_{C\equiv N}$ = 2166 and 2177 cm^{-1}) can be isolated.

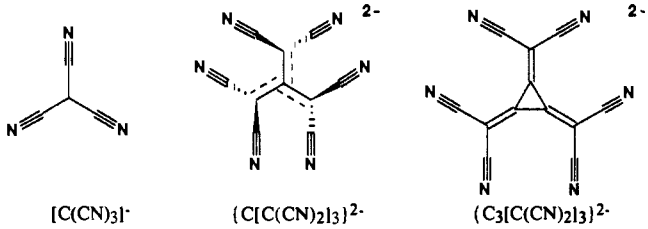

$Ni[S_2C_2(CF_3)_2]_2$ is a strong oxidant with formal reduction potentials of 0.92 and −0.12 V (versus SCE in MeCN)[11d] for the 0/− and −/2− redox processes, respectively. Thus, it seemed to be a suitable candidate to oxidize HOC to either $[HOC]^{4+}$-

(18) (a) Moller, C.; Plesset, M. S. *Phys. Rev.* **1934**, *46*, 618. (b) Pople, J. A.; Binkley, J. S.; Seeger, R. *Int. J. Quantum Chem. Symp.* **1976**, *10*, 1.

(19) The disproportionation constants for $2[HOC]^{n+} = [HOC]^{(n-1)+} + [HOC]^{(n+1)+}$ were estimated from the separation between $E°$ values at room temperature: n = 1, 3.9×10^{-9}; n = 2, 8.2×10^{-9}; n = 3, 4.1×10^{-7}. Therefore, it is unlikely that significant disproportionation occurs under these conditions. In addition, variable-temperature cyclic voltammetry indicated that disproportionation became even less favorable at lower temperatures (>210 K).

(20) Miller, J. S.; Dixon, D. A. *Science* **1987**, *235*, 871–873. Ward, M. D. *Organometallics* **1987**, *6*, 754.

Table II. Crystallographic Details for HOC, [HOC][BF_4], [HOC][TCNE], [HOC][F_3CSO_3], [HOC][BF_4]$_2$, [HOC][PF_6]$_2$, [HOC][$C(CN)_3$]$_2$, [HOC][$C[C(CN)_2]_3$], [HOC][$Ni[S_2C_2(CF_3)_2]_2$]$_2$, [HOC][PF_6]$_3$, [HOC][SbF_6]$_3$, and [HOC][SbF_6]$_4$·MeCN

compd	HOC	[HOC][BF_4][a]	[HOC]-[TCNE]	[HOC]-[F_3CSO_3]	[HOC][BF_4]$_2$	[HOC][PF_6]$_2$	[HOC]-[$C(CN)_3$]$_2$	[HOC][$C[C(CN)_2]_3$][c]	[HOC][$Ni[S_2C_4F_6]_2$]$_2$	[HOC][PF_6]$_3$	[HOC][SbF_6]$_3$	[HOC][SbF_6]$_4$·MeCN
formula	$C_{18}H_{24}N_6$	$C_{18}H_{24}N_6BF_4$	$C_{24}H_{24}N_{10}$	$C_{19}H_{24}F_3N_6SO_3$	$C_{18}H_{24}N_6B_2F_8$	$C_{18}H_{24}N_6P_2F_{12}$	$C_{26}H_{24}N_{12}$	$C_{28}N_{12}H_{24}$	$C_{34}H_{24}N_6S_8F_{24}$	$C_{18}H_{24}N_6P_3F_{18}$	$C_{18}H_{24}N_6Sb_3F_{18}$	$C_{20}H_{27}N_7Sb_4F_{24}$
formula wt	324.4	411.2	452.53	473.50	498.1	614.38	504.56	528.18	1346.5	759.32	1031.7	1308.4
space group	$P2_1/c$ (No. 14)	*Ibam* (No. 72)	$P\bar{1}$ (No. 2)	$P2_1/c$ (No. 14)	$P2_1/n$ (No. 14)	$P\bar{1}$ (No. 2)	$P\bar{1}$ (No. 2)	$P2_12_12_1$ (No. 19)	$P\bar{1}$ (No. 2)	$C2/m$ (No. 12)	$R\bar{3}m$ (No. 166)	$C2/m$ (No. 12)
a, Å	9.784 (2)	8.653 (1)	4.529 (1)	11.056 (4)	6.604 (1)	6.966 (2)	8.649 (2)	9.132 (6)	7.892 (1)	13.882 (3)	11.320 (2)	14.357 (1)
b, Å	9.384 (4)	9.948 (3)	10.859 (3)	10.093 (4)	10.929 (2)	8.915 (1)	8.994 (3)	33.747 (6)	12.345 (1)	11.339 (3)	11.320 (2)	11.652 (1)
c, Å	9.614 (8)	21.804 (3)	11.151 (3)	8.901 (4)	14.255 (3)	10.632 (2)	9.112 (2)	8.242 (8)	12.661 (1)	9.240 (3)	20.036 (3)	12.070 (1)
α, deg	90	90	88.62 (2)	90	90	100.45 (1)	103.35 (2)	90	105.35 (1)	90	90	90
β, deg	117.53 (3)	90	86.81 (2)	90.00 (4)	91.33 (1)	108.92 (2)	108.04 (2)	90	106.44 (1)	108.60 (2)	90	114.74 (1)
γ, deg	90	90	84.03 (2)	90	90	105.09 (1)	109.48 (2)	90	92.81 (1)	90	120	90
V, Å^3	782.7	1877	544.5	993.3	1028.6	577.0	589.5	2540	1131.4	1378.5	2223.5	1833.8
Z	2	4	1	2	2	1	1	4	1	2	3	2
ρ(calc), g cm^{-3}	1.373	1.46	1.380	1.583	1.608	1.768	1.421	1.382	1.976	1.829	2.311	2.369
crystal dimns, mm	0.38 × 0.08 × 0.50	0.08 × 0.50 × 0.76	0.18 × 0.15 × 0.45	0.38 × 0.02 × 0.45	0.30 × 0.20 × 0.30	0.30 × 0.20 × 0.30	0.37 × 0.23 × 0.52	0.10 × 0.05 × 0.45	0.18 × 0.35 × 0.50	0.17 × 0.17 × 0.17	0.27 × 0.22 × 0.28	0.20 × 0.30 × 0.36
temp, °C	−70	23	−70	−70	−70	−70	−70	−115	−70	−70	−70	−70
radiation	Mo Kα	Cu Kα	Mo Kα	Mo Kα	Mo Kα	Mo Kα	Mo Kα	Cu Kα	Mo Kα	Mo Kα	Mo Kα	Mo Kα
absorption coeff, cm^{-1}	0.81	9.8	0.83	2.18	1.42	2.99	0.87	6.87	13.25	3.53	28.66	30.82
transmission factors	none	none	none	none	none	none	0.96–0.99, ψ scan	0.82–1.27, DIFABS	0.49–1.31, DIFABS	0.90–0.96, ψ scan	0.21–1.41, DIFABS	0.49–0.59 ψ scan
scan mode	ω	ω–θ	ω	ω	ω	ω	ω	ω–2θ	ω	ω	ω	ω
2θ max, deg	55.0	156.0	55.0	55.0	55.0	55.0	55.0	120.1	60.0	48.0	60.0	60.0
total data measd	2066	1149	2616	4868	2616	2845	2906	3639	6831	2471	4424	2917
unique data with $(F_o)^2 > 3\sigma(F_o)^2$	673	428	906	343	1236	1527	1651	898	4680	635	656	2226
final no. of variables	109	75	154	65	202		220	161	337	220	48	169
weighting scheme	biweight[b]	unit weights	biweight[b]	biweight[b]	biweight[b]	biweight[b]	biweight[b]		biweight[b]	biweight[b]	biweight[b]	biweight[b]
R_u[d]	0.062	0.082	0.052	0.109	0.044	0.041	0.043	0.057	0.035	0.052	0.069	0.026
R_w[e]	0.053	0.086	0.048	0.111	0.043	0.043	0.044	0.059	0.040	0.045	0.058	0.028
largest resid, e Å^{-3}	0.22 (C1,N1)	0.24 (4)	0.24 (C10)	0.51 (F1)	0.25 (C1,C3)	0.27 (F5)	0.24	0.34	0.63	0.16	0.14	0.69

[a] Oneida Research Services (Whitesboro, NY). [b] $\propto[s^2(I) + 0.0009I^2]^{-1/2}$. [c] Molecular Structures Corp., College Station, TX. [d] $R_u = \sum(|F_o| - |F_c|)/\sum(|F_o|)$. [e] $R_w = \sum[w(|F_o| - |F_c|)^2]/\sum w(|F_o|)^2$.

Table III. Bond Distances, Å, for [HOC]^n (n = 0,1+,2+,3+,4+)

	distance, Å												
labeling	HOC[a]	[HOC]-[TCNE][a]	[HOC]-[F_3CSO_3][a]	[HOC]-[BF_4][b]	[HOC]-[BF_4]$_2$[a]	[HOC]-[PF_6]$_2$[a]	[HOC]-[$Ni[S_2C_4F_6]_2$]$_2$[a]	[HOC]-[$C[C(CN)_2]_3$][a]		[HOC]-[$C(CN)_3$]$_2$[a]	[HOC]-[PF_6]$_3$[b]	[HOC]-[SbF_6]$_3$[c]	[HOC]-[SbF_6]$_4$·MeCN[b]
N1–C1	1.414 (5)	1.387 (5)	1.394 (28)	1.371 (7)	1.340 (3)	1.335 (3)	1.351 (3)	1.31 (1)	1.33 (1)	1.335 (2)	1.326 (6)	1.317 (9)	1.303 (3)
N1–C4	1.449 (5)	1.445 (5)	1.409 (31)	1.464 (8)	1.468 (4)	1.455 (4)	1.444 (3)	1.46 (1)	1.47 (1)	1.459 (3)	1.477 (5)		1.478 (3)
N1–C5	1.448 (5)	1.443 (5)	1.435 (28)		1.461 (4)	1.457 (4)	1.455 (3)	1.46 (1)	1.45 (1)	1.469 (3)			
N2–C2	1.405 (5)	1.376 (5)	1.453 (29)	1.422 (9)	1.325 (4)	1.327 (3)	1.333 (3)	1.37 (1)	1.34 (1)	1.343 (2)	1.339 (7)		1.319 (4)
N2–C6	1.433 (5)	1.449 (5)	1.512 (33)		1.469 (4)	1.471 (4)	1.457 (3)	1.45 (1)	1.46 (1)	1.461 (3)			
N2–C7	1.446 (5)	1.457 (5)	1.442 (30)		1.467 (4)	1.455 (4)	1.464 (3)	1.47 (1)	1.48 (1)	1.457 (3)			
N3–C3	1.428 (5)	1.386 (5)	1.388 (26)		1.411 (3)	1.415 (3)	1.387 (3)	1.38 (1)	1.42 (1)	1.407 (2)			
N3–C8	1.430 (5)	1.452 (5)	1.510 (28)		1.447 (4)	1.462 (4)	1.457 (3)	1.43 (1)	1.45 (1)	1.467 (3)			
N3–C9	1.441 (5)	1.446 (5)	1.522 (32)		1.461 (4)	1.456 (4)	1.453 (3)	1.46 (1)	1.45 (1)	1.462 (3)			
C1–C2	1.405 (5)	1.424 (5)	1.421 (31)	1.382 (6)	1.476 (4)	1.478 (4)	1.455 (3)	1.45 (1)	1.48 (1)	1.473 (3)	1.417 (4)		1.434 (3)
C1–C3a	1.388 (5)	1.386 (5)	1.384 (27)		1.384 (4)	1.384 (4)	1.391 (3)	1.39 (1)	1.42 (1)	1.400 (3)			
C2–C3	1.399 (5)	1.417 (5)	1.390 (29)		1.409 (4)	1.396 (4)	1.406 (3)	1.40 (1)	1.40 (1)	1.389 (3)			
C4–C9a	1.496 (6)	1.497 (6)	1.517 (34)		1.514 (4)	1.503 (5)	1.502 (4)	1.51 (1)	1.50 (1)	1.509 (3)			
C5–C6	1.498 (6)	1.505 (6)	1.476 (32)		1.498 (4)	1.480 (5)	1.496 (4)	1.50 (1)	1.48 (1)	1.485 (3)			
C7–C8	1.488 (6)	1.491 (6)	1.536 (34)		1.509 (4)	1.499 (5)	1.497 (4)	1.54 (1)	1.52 (1)	1.506 (3)			
N1–C2												1.446 (10)	
N1–C3				1.426 (8)							1.455 (5)		1.464 (3)
N2–C5				1.452 (8)							1.457 (5)		1.475 (3)
C1–C1				1.444 (6)							1.439 (7)	1.419 (7)	1.439 (4)
C2–C2												1.520 (21)	
C3–C3				1.50 (1)							1.524 (7)		1.521 (5)
C4–C5				1.48 (1)							1.499 (6)		1.514 (4)

[a] Figure 2a. [b] Figure 2b. [c] Figure 2c.

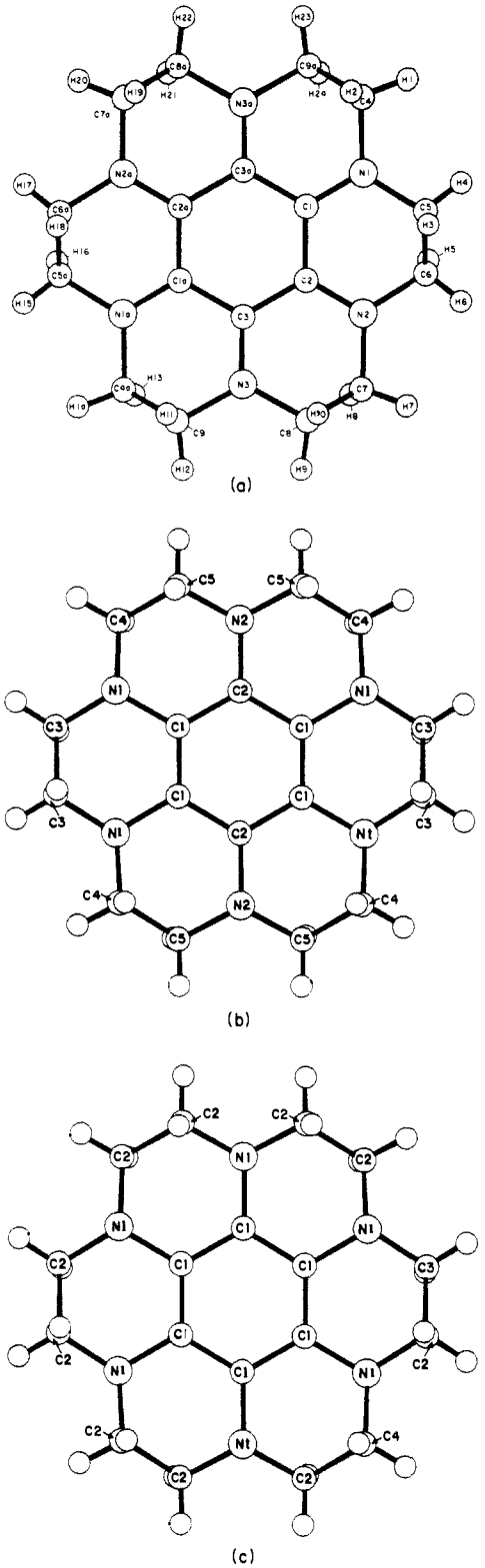

Figure 2. (a) Atom labeling for HOC in HOC, [HOC][TCNE], [HOC][F_3CSO_3], [HOC][BF_4]$_2$, [HOC][$C(CN)_3$]$_2$, [HOC]$^{2+}${[Ni[S_2C_2-(CF_3)$_2$]$_2$]$^{-}$}$_2$, [HOC]{C[$C(CN)_2$]$_3$}, and [HOC][PF_6]$_2$; (b) [HOC][BF_4], [HOC][PF_6]$_3$, and [HOC][SbF_6]$_4$·MeCN; and (c) [HOC][SbF_6]$_3$.

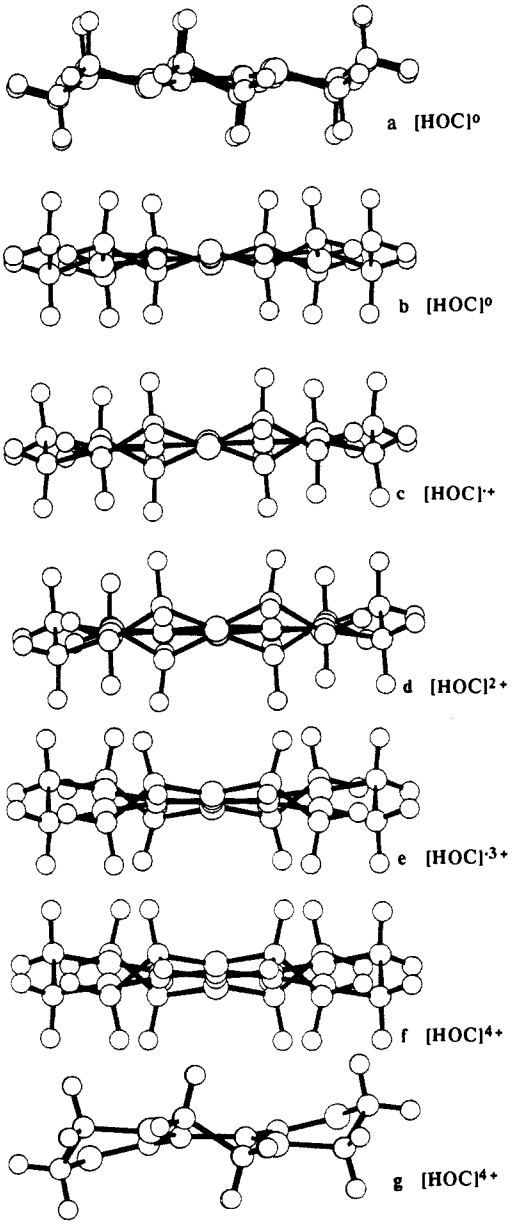

Figure 3. Side view of [HOC]^{n} (n = 0 (a, b); 1+, [HOC][BF_4] (c); 2+, [HOC][BF_4]$_2$ (d); 3+, [HOC][SbF_6]$_3$ (e); 4+, [HOC][SbF_6]$_4$·MeCN (f, g)].

{[Ni[$S_2C_2(CF_3)_2$]$_2$]$^{2-}$}$_2$ or [HOC]$^{4+}${[Ni[$S_2C_2(CF_3)_2$]$_2$]$^{\cdot-}$}$_4$. However, with either 2 or 4 equiv of Ni[$S_2C_2(CF_3)_2$]$_2$, only [HOC]$^{2+}${[Ni[$S_2C_2(CF_3)_2$]$_2$]$^{\cdot-}$}$_2$ could be isolated.

In contrast to the [HOC]^{n} salts (n = 1+ and 2+), the solubility of HOC is limited to CH_2Cl_2, with which HOC slowly reacts to form [HOC]$^{\cdot+}$, as evidenced by NMR and EPR spectra. The solubility of the [HOC]$^{n+}$ (n = 3+, 4+) cations is very low in CH_2Cl_2, but in contrast to HOC, the 1+, 2+, 3+, and 4+ salts are soluble in MeCN. Crystals of all salts suitable for single-crystal X-ray diffraction were successfully grown by diethyl ether (or CH_2Cl_2) diffusion into a MeCN solution of the cation.

Crystal Structures of HOC, [HOC][BF_4], [HOC][TCNE], [HOC][F_3CSO_3], [HOC][BF_4]$_2$, [HOC][PF_6]$_2$, [HOC][$C(CN)_3$]$_2$, [HOC]{C[$C(CN)_2$]$_3$}, [HOC]{Ni[$S_2C_2(CF_3)_2$]$_2$}$_2$, [HOC][PF_6]$_3$, [HOC][SbF_6]$_3$, and [HOC][SbF_6]$_4$·MeCN. The C–C and C–N bond distances are given in Table III. Averaged chemically equivalent distances are given in Table IV. The atom labeling is given in Figure 2. Representative side views for each value of n are shown in Figure 3. Stereoviews of the unit cells are included as supplementary material. The anions are not discussed since their structural features have been previously reported.

HOC crystallizes in the monoclinic $P2_1/c$ space group. The atom labeling can be found in Figure 2a. The solid comprises ribbons of HOC with adjacent HOC planes being canted by 60°. The shortest contact between adjacent HOC's is between hydrogens that are separated by 2.54 Å.

[**HOC**]$^{\cdot+}$[BF_4]$^{-}$ crystallizes in the orthorhombic *Ibam* space group. The atom labeling can be found in Figure 2b. Like HOC, the solid is composed of ribbons of [HOC]$^{\cdot+}$ with adjacent cations canted by 60°. Since the F's are disordered, the N···F interaction distance cannot be uniquely described. The N···B distances are

Table IV. Average Bond Lengths, Å, for $[HOC]^n$ (n = 0,1+,2+,3+,4+)

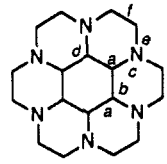

compd	obs/calc	*a*	*b*	*c*	*d*	*e*	*f*
HOC	obs	1.397	1.397	1.416	1.416	1.442	1.492
HOC	calc	1.401 (1.37)[a]	1.401 (1.37)[a]	1.453 (1.02)[a]	1.453 (1.02)[a]	1.474	1.537
$[HOC][BF_4]$	obs	1.382	1.444	1.371	1.422	1.449	1.487
[HOC][TCNE]	obs	1.410	1.410	1.383	1.383	1.448	1.499
$[HOC][F_3CSO_3]$	obs	1.40	1.40	1.41	1.41	1.47	1.51
$[HOC]^{\bullet+}$	calc	1.404	1.463	1.392	1.459	1.478	1.536
$[HOC][BF_4]_2$	obs	1.397	1.476	1.333	1.415	1.462	1.507
$[HOC][PF_6]_2$	obs	1.390	1.478	1.332	1.411	1.459	1.494
$[HOC][C(CN)_3]_2$	obs	1.395	1.473	1.339	1.407	1.463	1.500
$[HOC]\{C[C(CN)_2]_3\}$	obs	1.40	1.46_5	1.34	1.40	1.46	1.51
$[HOC]\{Ni[S_2C_2(CF_3)_2]_2\}_2$	obs	1.398	1.455	1.342	1.387	1.455	1.497
$[HOC]^{2+}$ av[b]	obs	1.395	1.471	1.337	1.405	1.460	1.500
$[HOC]^{2+}$ **1**	calc	1.401	1.522	1.349	1.458	1.489	1.537
$[HOC]^{2+}$ **2**	calc	1.491	1.353	1.423	1.318	1.482	1.536
$^3[HOC]^{2+}$	calc	1.429 (1.23)[a]	1.429 (1.23)[a]	1.383 (1.22)[a]	1.383 (1.22)[a]	1.480	1.539
$[HOC][PF_6]_3$	obs	1.417	1.439	1.326	1.339	1.463	1.512
$[HOC][SbF_6]_3$	obs	1.419	1.419	1.317	1.317	1.446	1.520
$[HOC]^{\bullet3+}$	calc	1.44	1.49	1.33	1.38	1.49	1.53
$[HOC][SbF_6]_4$	obs	1.436	1.436	1.318	1.318	1.472	1.518
$[HOC]^{4+}$	calc	1.475 (1.11)[a]	1.475 (1.11)[a]	1.330 (1.52)[a]	1.330 (1.52)[a]	1.506	1.542

[a] Calculated total bond order (see text). [b] Average excludes data from $[HOC]\{C[C(CN)_2]_3\}$.

4.84 and 4.90 Å for the four equivalent N1's and 6.10 Å for the pair of N2's. Another monoclinic polymorph was also isolated; however, the structure is disordered with a large R_w of 0.131 and is not reported here.

$[HOC]^{\bullet+}[TCNE]^{\bullet-}$ crystallizes in the triclinic $P\bar{1}$ space group. Atom labeling for the cation can be found in Figure 2a. The radical ions form parallel segregated chains, with the cation planes being separated by 4.00 Å and the $[TCNE]^{\bullet-}$ planes by 3.85 Å.

$[HOC]^{\bullet+}[F_3CSO_3]^-$ crystallizes in the monoclinic $P2_1/c$ space group. Atom labeling for the cation can be found in Figure 2a. Like HOC and $[HOC]^{\bullet+}[BF_4]^-$, the solid comprises chains of $[HOC]^{\bullet+}$ with adjacent cations canted by ~60°. Due to disorder across a crystallographic inversion center of the triflate anion (modeled by hexafluoroethane), the anion–cation distances do not warrant discussion. This is the structure of the poorest quality reported in this paper, and a discussion of the bond distances is not warranted.

$[HOC]^{2+}\{[BF_4]^-\}_2$ crystallizes in the monoclinic $P2_1/c$ space group. Atom labeling for the dication can be found in Figure 2a. The solid is composed of slipped chains of $[HOC]^{2+}$, with the $[BF_4]^-$ anions located between the cations. The N···B separations are N1···B 4.43 Å, N2···B 4.08 and 4.90 Å, and N3···B 4.09 Å. The N1···F distances range from 3.25 to 5.72 Å, the N2···F distances range from 3.76 to 5.76 Å, and the N3···F distances range from 3.02 to 5.01 Å. Thus, the charge environment for all N's is essentially equivalent.

$[HOC]^{2+}\{[PF_6]^-\}_2$ crystallizes in the triclinic $P\bar{1}$ space group. Atom labeling for the dication can be found in Figure 2a. The solid is composed of slipped chains of $[HOC]^{2+}$, with the $[PF_6]^-$ anions located between the cations. The shortest N1···P separations are 5.02 and 5.12 Å. The shortest N2···P distances are 4.44, 4.67, and 4.86 Å, and the shortest N3···P contact is 4.24 Å. There are six N···F distances below 5 Å, with the shortest being 4.21 Å, and seven N2···F distances less than 5 Å, with the shortest being 4.17 Å. For the N2···F distances, five are less than 5 Å—the shortest being 4.24 Å.

$[HOC]^{2+}\{[C(CN)_3]^-\}_2$ crystallizes in the triclinic $P\bar{1}$ space group. Atom labeling for the dication can be found in Figure 2a. The solid is composed of parallel alternating $\cdots D^{2+}A^-A^-D^{2+}A^-A^-\cdots$ chains of $[HOC]^{2+}\{[C(CN)_3]^-\}_2$, with each cation being surrounded by eight anions. The $[C(CN)_3]^-$ and $[HOC]^{2+}$ ions are canted with respect to each other by 9°. A $[C(CN)_3]^-$ anion is situated above and below the C_6 ring such that the central C is essentially equidistant (3.71–3.89 Å) from the ring carbons and is 3.52 Å from the ring centroid. From a view normal to the C_6 ring, the anion/cation pair appears to have C_3 symmetry. The N···N separation between the anion above and below the C_6 ring and the C_6-ring N's range from 3.23–3.96 Å, whereas the shortest N···N separation between the C_6-ring N's and the other anion N's are 3.44 and 3.38 Å.

$[HOC]^{2+}\{Ni[S_2C_2(CF_3)_2]_2^{\bullet-}\}_2$ crystallizes in the triclinic $P\bar{1}$ space group. Atom labeling for the dication can be found in Figure 2a. The asymmetric unit is composed of a half $[HOC]^{2+}$ and two equivalent half $Ni[S_2C_2(CF_3)_2]_2^{\bullet-}$ anions. Both half-anions are chemically equivalent. The solid comprises alternating donor/acceptor ···DADA··· chains. The second $Ni[S_2C_2(CF_3)_2]_2^{\bullet-}$ radical anion lies in a ···AAA··· chain orthogonal to the ···DADA··· chains. The shortest Ni···Ni distance is 6.18 Å. The shortest $Ni[S_2C_2(CF_3)_2]_2^{\bullet-}\cdots$ $[HOC]^{2+}$ interactions are two C···F bonds of 3.02 and 3.18 Å.

$[HOC]^{2+}\{C[C(CN)_2]_3\}^{2-}$ crystallizes in an acentric orthorhombic $P2_12_12_1$ space group; however, the absolute configuration could not be determined because of the absence of heavy atoms. Atom labeling for the dication can be found in Figure 2a. The crystals scattered poorly, and the number of data were increased by using lower temperatures (−115 °C) and a high intensity source (12 kW). The structure was refined isotropically because the thermal parameters of several atoms was refined to unreasonable values during anisotropic refinement. As a consequence, the data/parameter ratio increased significantly. The space group was determined to be $P2_12_12_1$ on the basis of the systematic absences [$h00$, $h \neq 2n$; $0k0$, $k \neq 2n$; and $00l$, $l \neq 2n$] and the successful solution and refinement of the structure. The poor scattering and broad diffraction peaks led to relatively large errors in the unit-cell constants. This in turn led to large estimated standard deviations in the bond distances and angles. This is particularly important for the short axes [a = 9.132 (6) Å and c = 8.242 (8) Å]. Consequently, this structure was not included in the determination of average values. However, it does show the same trends observed for the other $[HOC]^{2+}$ salts, and its inclusion would only alter the averages that we report for $[HOC]^{2+}$ by ≤0.002 Å.

The solid comprises parallel chains of alternating $[HOC]^{2+}$ and $\{C[C(CN)_2]_3\}^{2-}$ ions. The anion is nonplanar, with each $C(CN)_2$ group twisted in a propeller fashion, and sits midway between the

cations along *b*. Mean planes through the C_4 moieties are parallel to each other and separated by 7 Å. A $\{C[C(CN)_2]_3\}^{2-}$ anion is offset above and below the C_6 ring of $[HOC]^{2+}$ such that the central C is 4.12 Å above a C_6-ring C and 4.25 Å from the N bonded to that C in the dication. Anion N's are 3.15, 3.34, and 3.85 Å from C_6-ring C's and 3.64 Å from an N in the dication.

$[HOC]^{\bullet 3+}\{[PF_6]^-\}_3$ crystallizes in the monoclinic $C2/m$ space group. Atom labeling for the trication can be found in Figure 2b. The solid comprises slipped chains of $[HOC]^{\bullet 3+}$ with the $[PF_6]^-$ anions located between the cations. The N···P separations are N(1)···P 4.65, 4.83, and 4.79 Å and N(2)···P and N(3)···P 3.99, 4.42, and 4.60 Å. There are six N(1)···F and N(3)···F distances below 4 Å, with the shortest being 3.27 Å. Two N(2)···F distances less than 4 Å (3.38 and 3.89 Å) are also present in the structure. There is a $[PF_6]^-$ anion located 3.8 Å above and below the C_6 ring essentially over the ring centroid. The charge environment around all N's is essentially the same.

$[HOC]^{\bullet 3+}\{[SbF_6]^-\}_3$ crystallizes in the hexagonal $R\bar{3}m$ space group. Atom labeling for the cation can be found in Figure 2c. The ethylene bridges show high thermal motions and one $[SbF_6]^-$ is disordered. The solid is composed of layers of isolated $[HOC]^{\bullet 3+}$ cations with $[SbF_6]^-$ anions above and below (3.93 Å) the C_6-ring center and above and below trigonal sites adjacent to three cations. The shortest F···C_6 ring C distance is 2.89 Å. The $[SbF_6]^-$ anion above the C_6 ring has Sb···N distances of 4.61 and 4.96 Å. In addition, other N···Sb separations are 4.02 and 4.83 Å.

$[HOC]^{4+}\{[SbF_6]^-\}_4 \cdot MeCN$ crystallizes in the monoclinic $C2/m$ space group. Atom labeling for the tetracation can be found in Figure 2b. The solid is composed of slipped chains of isolated $[HOC]^{4+}$ cations, with the $[SbF_6]^-$ anions separating the cations. There are $[SbF_6]^-$ anions 3.87 Å above and below the C_6 ring, which are 4.52–4.95 Å from the N's. In addition, the N1···Sb separations are 4.78 and 4.80 Å, and the N2···Sb distances are 4.68 Å. There are six N1···F and N2···F distances below 4 Å, with the shortest being 3.25 Å. The charge environment for all N's is essentially equivalent.

Structures of $[HOC]^n$ (n = 0, 1+, 2+, 3+, 4+). HOC is a substituted benzene ring with D_{3d} symmetry. The benzene ring has normal C_6-ring C–C benzene distances. The C_6-ring C–N bond distances are those expected for an amino-substituted benzene (e.g., for *p*-diaminobenzene r(C–N) = 1.422 Å in the gas and 1.416 Å in the crystal[21a]). The N–C_H (C_H refers to the CH_2 carbon) bonds are slightly shorter than the value of 1.452 Å observed for $N(CH_3)_3$.[21b] The C_H–C_H bonds (with staggered hydrogens) have shorter bond lengths (1.49 Å) than the normal C–C alkane bond length of 1.54 Å. This shortening is most likely due to geometrical constraints imposed by the bonds in the various rings.

A simple Hückel model for HOC (borne out by the ab initio calculations described below) is useful in describing the structural variations in its various oxidation states. The "π orbitals" of HOC can be formally generated by adding the π orbitals of the N lone pairs to the benzene π orbitals. (In the illustration below, the energy scales are not the same.) The exact mixing depends on

C_6-ring π orbitals N lone-pair orbitals

a variety of factors such as overlap, electron repulsion, etc. The HOMO of HOC is degenerate (e_{1g} symmetry) and has significant density on both C and N. Removal of one electron in a vertical process leads to an $[\,]e^3$ configuration, a ^2E electronic state, and

Scheme II

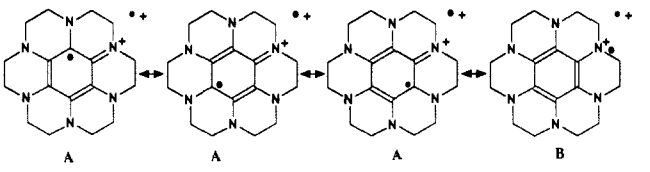

A A A B

[HOC]$^{\bullet+}$ Resonance Structures

removal of three electrons leads to an $[\,]e^1$ configuration, also a ^2E state. (The brackets denote the underlying occupied orbitals.) Removal of two electrons in a vertical process to generate the dication produces a $[\,]e^2$ orbital configuration. For a triplet coupling of the two electrons, a ^3A state is expected, whereas for a singlet coupling an ^1E or ^1A state would be anticipated. The ^1A state should be quite high in energy and may be ignored. The ^1E state of the dication and the ^2E states of the mono- and trications must, of course, undergo Jahn–Teller distortions to break the orbital degeneracy. For the dication, this distortion leads to a closed shell singlet. The two most likely Jahn–Teller distortions are those shown below for the dication; one distortion leads to two cyanine cations connected by C–C single bonds, **1**, and the other leads to the formation of **2** which resembles the *p*-phenylenediiminium dication. If the Jahn–Teller distortions for the ^1E state of the dication are strong enough, then the distorted, nondegenerate singlet state can lie below the delocalized triplet state with 3-fold symmetry.

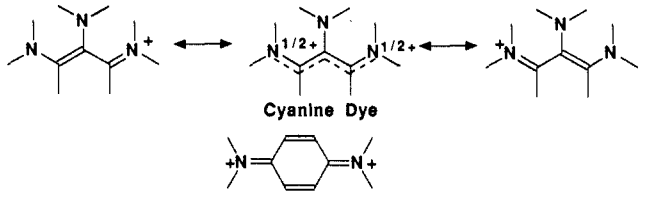

Cyanine Dye

N,N,N',N'-Tetramethyl-*p*-phenylenediiminium dication

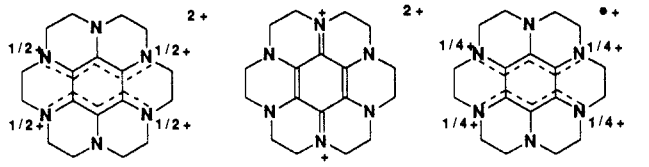

1 2 3

[HOC]$^{\bullet+}$. The three crystal structures for $[HOC]^{\bullet+}$ show different features. We focus on the structures with $[BF_4]^-$ and $[TCNE]^{\bullet-}$ counterions since they are the best structure determinations. With the $[BF_4]^-$ ion (localized charge), the structure of $[HOC]^{\bullet+}$ clearly shows a distortion away from ideal D_{3d} symmetry to a C_{2h} structure. The distorted structure resembles two cyanine moieties coupled by C–C single bonds, **3**; i.e., there are four short C_6-ring C–C and C_6-ring C–N distances and two long C_6-ring C–C and C_6-ring C–N distances. Distribution of the negative charge over more centers in the anion (e.g., $[TCNE]^{\bullet-}$) should result in less polarization of the cation. Accordingly, the C_6-ring C–C and C–N bonds are more nearly equivalent in the $[TCNE]^{\bullet-}$ salt; i.e., the static Jahn–Teller distortion is smaller. This points out how static Jahn–Teller distortions[22] depend on the crystal environment. The average C_6-ring C–C bond distances are larger in the monocation compared to the neutral molecule, whereas the average C_6-ring C–N bond distances are significantly smaller.

Scheme II depicts 4 of the 24 resonance structures that could stabilize $[HOC]^{\bullet+}$. Type A structures have the unpaired electron on the C_6 ring, whereas type B have the unpaired electron on a nitrogen. These resonance structures are similar to those invoked for the stabilization of the *N,N,N',N'*-tetramethyl-*p*-phenylene-

(21) (a) Colapiefro, M.; Domenciano, A.; Portalone, G.; Schultz, G.; Hargittai, I. *J. Phys. Chem.* **1987**, *81*, 1728. (b) Tsuboi, M.; Hirakawa, A. Y.; Tamagake, K. *J. Mol. Spectrosc.* **1967**, *22*, 272.

(22) Hargittai, I.; Hargittai, I. *Symmetry Through the Eyes if a Chemist*; VCH Publishers: New York, 1987; pp 273–277.

Scheme III

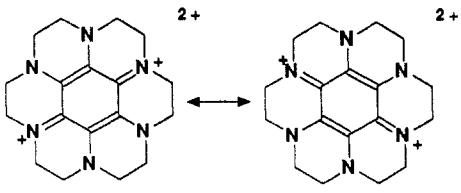

5a 5b

$[HOC]^{2+}$ Resonance Structures

diamine radical cation, $[TMPD]^{\bullet+}$.[23] Assuming equal contributions of the A and B resonance structures, the unpaired electron density would on the average be 3 times greater on the C_6-ring carbon than on a nitrogen in this simple model. Of course, since B has aromatic character, it will be dominant and the ratio of spin on C to the spin on N will decrease. Molecular orbital calculations (vide infra) are consistent with the spin being delocalized over all of the C_6-ring carbons and nitrogen centers with slightly more spin on the nitrogens.

$[HOC]^{2+}$. Four independent single-crystal X-ray structures of this dication have been determined at −70 °C; one low-quality structure at −115 °C (vide supra) was also determined. The dication has distinct short and long C_6-ring C–N and C_6-ring C–C bonds. For the four −70 °C structures, the average short C_6-ring C–N and C_6-ring C–C distances range from 1.332 to 1.342 and 1.390 to 1.398 Å and average 1.337 and 1.395 Å, respectively. The average long C_6-ring C–N and C_6-ring C–C distances range from 1.387 to 1.415 and from 1.455 to 1.478 Å and average 1.405 and 1.471 Å, respectively. The differences between the short and long C_6-ring C–C and C_6-ring C–N distances range from 19 to 26 times the observed estimated standard deviation. Thus, the observed structure clearly shows a pronounced C_{2h} distortion away from the idealized D_{3d} symmetry. The four short C_6-ring C–C and C_6-ring C–N bonds and two long C_6-ring C–C and C_6-ring C–N bonds are again consistent with a pair of independent cyanine moieties coupled by C–C single bonds, **1**. For example, in the simple cyanine dye 1,3-bis(dimethylamino)trimethinium perchlorate, **4b**, the C–C and C–N bonds average 1.381 and 1.308

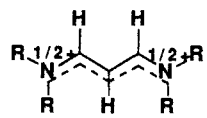

4a (R =H); **4b** (R = Me)

Å, respectively,[24] which are comparable to the corresponding short bond lengths for $[HOC]^{2+}$ (1.395 and 1.337 Å). The dication in a variety of crystalline environments clearly shows a Jahn–Teller distortion (static) which removes the orbital degeneracy and leads to an electronic singlet ground state consistent with magnetic susceptibility and EPR measurements (vide infra). Electrostatic

Scheme IV

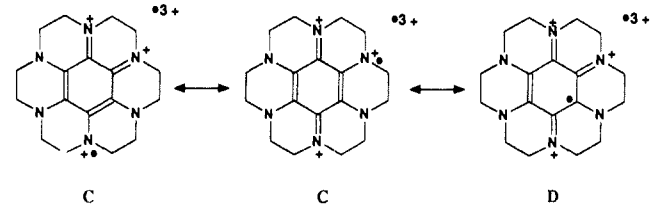

C C D

$(HOC)^{3+}$ Resonance Structures

interactions associated with ion pairing presumably play a role in determining if and exactly how $[HOC]^{2+}$ will distort since in some very special environments, i.e., certain frozen solutions, $[HOC]^{2+}$ can exist as a ground-state triplet or very close to it.[7,34]

Resonance structures **5** for $[HOC]^{2+}$ are presented in Scheme III. Since the structure in the solid state has effectively C_{2h} symmetry, the delocalization of charge is best described at the valence bond level as the sum of **5a** and **5b** and not by **6**, as

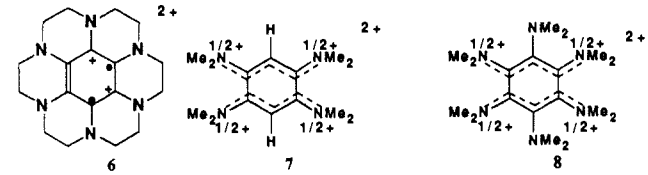

6 7 8

previously drawn.[7a] This sum also represents the Jahn–Teller distortion, leading to the two coupled cyanine dye moieties. A similar distortion has recently been reported for the dication salts of 1,2,4,5-tetrakis(dimethylamino)benzene, **7**,[25a] and hexakis(dimethylamino)benzene, **8**,[25b] although the C_6 rings, as well as the C_6N_4 or C_6N_6 moieties, are nonplanar for these substituted benzene dications. Here there are no constraints due to the CH_2–CH_2 bridging groups on the nitrogens.

The structure of $[HOC]^{2+}\{[TCNE]^{-}\}_2$ has not been determined since suitable crystals were not available. This salt has characteristic infrared $\nu_{C\equiv N}$ absorptions at 2159 s, 2175 s, and 2190 m cm^{-1}. The infrared frequencies suggest the presence of diamagnetic $[TCNE]_2^{2-}$ which possesses characteristic infrared $\nu_{C\equiv N}$ absorptions at 2160 s, 2169 s, and 2190 m cm^{-1} in the solid.[26] The dimer dianion has been characterized by single-crystal X-ray diffraction[26] and is diamagnetic according to EPR and magnetic susceptibility data, vide infra.

$[HOC]^{\bullet 3+}$. The two structures determined for $[HOC]^{\bullet 3+}$ show significant differences. The $[SbF_6]^-$ containing structure is disordered, and only an average structure could be refined (space group imposes $\bar{3}m$ symmetry on the cation) precluding any observation of static Jahn–Teller distortions. The structure determined for the $[PF_6]^-$ salt, however, clearly shows the expected static Jahn–Teller distortion **9** with four short and two long C_6-ring

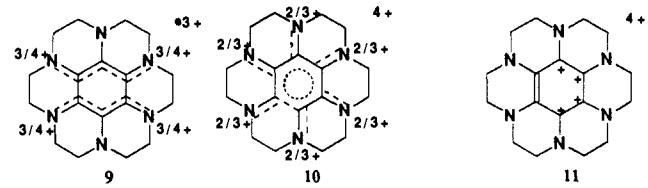

9 10 11

C–C and C_6-ring C–N bonds. The differences in bond lengths are not as pronounced as those seen in $[HOC]^{\bullet+}$ or $[HOC]^{2+}$. Three of the 18 resonance structures for $[HOC]^{\bullet 3+}$ are presented in Scheme IV; types C have the unpaired electron on the nitrogens, and type D has the unpaired electron on the ring carbons. Assuming equal contributions of the C and D structure types, on the average there would be twice as much unpaired electron density on the nitrogens than on the C_6-ring carbons. Molecular orbital calculations (vide infra) are consistent with the spin being delocalized over all of the benzene carbon and nitrogen centers and, on the average, place more spin density on the nitrogens, consistent with the simple valence bond model.

(23) Bent, R. L.; Dessloch, J. C.; Duennebier, F. C.; Fassett, D. W.; Glass, D. B.; James, T. H.; Julian, D. B.; Ruby, W. R.; Sterner, J. H.; Thirtle, J. R.; Vittum, P. W.; Weissberger, A. *J. Am. Chem. Soc.* **1951**, *73*, 3100.
(24) Mathews, B. W.; Steinkamp, R. E.; Colman, P. M. *Acta Crystallogr.* **1973**, *B29*, 449.
(25) (a) Elbl, K.; Krieger, C.; Staab, H. A. *Angew. Chem., Int. Ed. Engl.* **1986**, *25*, 102; *Angew. Chem.* **1986**, *98*, 1024. (b) Chance, J. M.; Kahr, B.; Buda, A. B.; Toscano, J. P.; Mislow, K. *J. Org. Chem.* **1988**, *53*, 3226–3232. Siegal, J.; Calabrese, J. C.; Miller, J. S. Unpublished work.
(26) Miller, J. S.; O'Hare, D. M.; Chackraborty, A.; Epstein, A. J. *J. Am. Chem. Soc.* **1989**, *111*, 7853–7860.
(27) Shimanouchi, T. *Tables of Molecular Vibrational Frequencies*; NSRDS-NBS 39; U.S. Government: Washington, DC, 1972; Vol. 1, p 152.
(28) Dixon, D. A.; Eaton, D. F. Unpublished results.
(29) Miller, J. S.; Glatzhofer, D. T. Submitted.
(30) Herzberg, G. *Electronic Spectra and Electronic Structure of Polyatomic Molecules*; van Nostrand-Reinhold: New York, 1965; p 555.
(31) Malhotra, S. S.; Whiting, M. C. *J. Chem. Soc.* **1960**, 3812. Gold, H. *Angew. Chem.* **1960**, *72*, 956.
(32) Boudreaux, E. A.; Mulay, L. N. *Theory and Applications of Molecular Paramagnetism*; John Wiley and Sons: New York, 1976; p 497 ff.
(33) Gabe, E. J.; Morton, J. R.; Preston, K. F.; Dixon, D. A.; Krusic, P. J.; Wasserman, E.; Miller, J. S. *J. Phys. Chem.* **1989**, *93*, 5337.
(34) Krusic, P. J. et al. To be published.

Scheme V

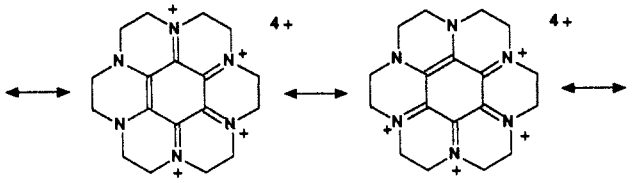

[HOC]$^{4+}$ Resonance Structures

[HOC]$^{4+}$. The simplified Hückel model predicts that removal of four electrons from HOC should lead to a closed shell singlet. However, the lost electrons are from molecular orbitals that are a mixture of atomic orbitals on the C_6-ring carbons and on the nitrogens and removal of four electrons from HOC could cause the orbital ordering to change, leading to an e^2 occupancy and a triplet for [HOC]$^{4+}$. Magnetic susceptibility measurements (vide infra) showed that [HOC]$^{4+}$ is diamagnetic between 2.2 and 320 K, and there is no evidence of a triplet-state contribution. Although the $4n + 2$ electron counting rule can be applied to substituted benzenes, it is inappropriate for determining the charge distribution of [HOC]$^{4+}$. The $4n + 2$ rule would place four positive charges on the benzene ring. However, the C_6-ring C–N bonds are very short, and the excess positive charges are clearly in the regions of the nitrogens, Scheme V. These [6]radialene structures have the positive charges on N, **10**, not on the C_6-ring C, **11**, as previously drawn.[7a]

Bond Distances. To visualize the regions of the molecule that are electron deficient after oxidation, the C_6-ring C–C and C_6-ring C–N bond distances are plotted as a function of n, Figure 4 (see also Table IV). Oxidation leads to removal of electrons from the C_6-ring bonding orbitals and from the nitrogen lone pairs. In general the average C_6-ring C–C bond distance increases with n, indicating a decrease in bond order, Figure 4a; whereas the average C_6-ring C–N distance decreases with n, indicating an increase in bond order, Figure 4b. The increase in charge in the C_6-ring C–N region leads to more iminium character in the C–N bonds and a shorter bond length. The pattern of distortion for the n = 1+, 2+, and 3+ ions is also evident in parts a and b of Figure 4. The largest divergence occurs for n = 2+, where the Jahn–Teller distortion is greatest. All crystal structures we have investigated for n = 1+, 2+, and 3+ with a variety of anions that lack the symmetry-imposed equivalence of atomic positions exhibit atomic positions expected for the Jahn–Teller distortion. Although environmental crystal effects cannot be rigorously excluded, the preponderance of this behavior strongly suggests that the observed distortions arise from an intrinsic Jahn–Teller electronic distortion.

Planarity. The structures of [HOC]^n (n = 0, 1+, 2+, 3+, 4+) have the common feature of an essentially planar C_6N_6 core with increased puckering of the NCH_2CH_2N moieties with increasing n, Table V and Figure 3. The puckering conformation for all structures determined is illustrated by **12a**, and evidence does not

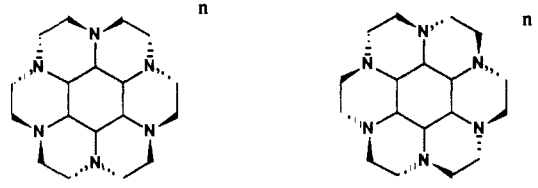

12a **12b**

exist for **12b**. Indeed **12b** is predicted to be 29.5 kcal/mol higher in energy than **12a** at the SCF (HF/STO-3G) level. The C_6 ring is essentially planar for all values of n with average deviations of any C_6-ring carbon from the least-squares plane of <0.01 Å for n = 0, 1+, and 2+ and ~0.03 and 0.05 Å for n = 3+ and 4+, respectively. The deviations of any C_6N_6 atom from their least-squares planes are also small for n = 0, 1+, 2+, but are more substantial (0.11 and 0.15 Å) for n = 3+ and 4+, respectively. The C_2H_4 groups are clearly out the C_6N_6 plane by ~0.32 Å for n = 0, 1+, and 2+ and 0.43 and 0.46 Å for n = 3+ and 4+, respectively.

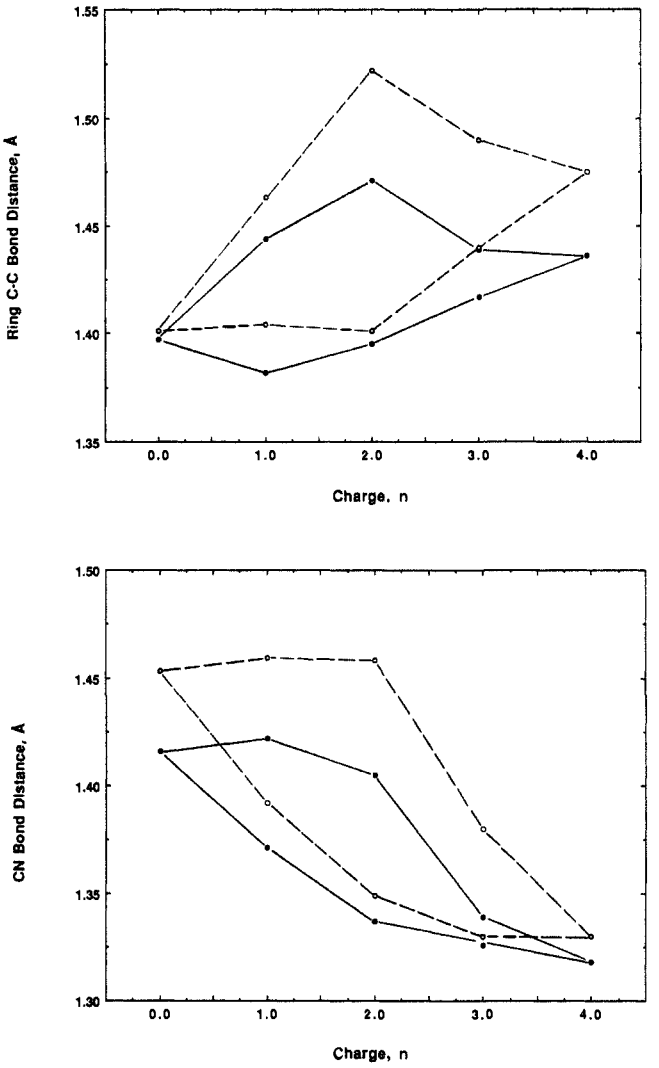

Figure 4. C_6-ring C–C (a, top) and C–N bond distances (b, bottom) as a function of n. Calculated values (O). The distances for [HOC]$^{2+}$ correspond to an average. The solid and dashed lines are a guide for the eye.

Table V. Average Deviations from Least-Squares Planes

	C_6 least-squares plane			C_6N_6 least-squares plane	
n, [HOC]^n; anion	C_6 ring	N_6 core	C_2H_4 groups	C_6N_6 core	C_2H_4 groups
0	±0.013	±0.116	±0.320	±0.065	±0.341
1+; $[BF_4]^-$	±0.009	±0.017	±0.321	±0.014	±0.321
1+; $[F_3CSO_3]^-$	±0.001	±0.041	±0.322	±0.020	±0.372
1+; $[TCNE]^{\bullet-}$	±0.009	±0.108	±0.337	±0.039	±0.385
1+; av	±0.006	±0.055	±0.327	±0.030	±0.379
2+; $[PF_6]^-$	±0.012	±0.107	±0.323	±0.040	±0.347
2+; $[BF_4]^-$	±0.013	±0.095	±0.361	±0.038	±0.360
2+; $[C(CN)_3]^-$	±0.008	±0.092	±0.357	±0.034	±0.356
2+; $\{Ni[S_2C_4F_6]_2\}^-$	±0.009	±0.084	±0.349	±0.033	±0.353
2+; $\{C[C(CN)_2]_3\}^{2-}$	±0.011	±0.064	±0.352	±0.032	±0.351
2+; av	±0.011	±0.088	±0.348	±0.035	±0.353
3+; $[PF_6]^-$	±0.034	±0.190	±0.430	±0.111	±0.430
3+; $[SbF_6]^-$	±0.043	±0.212	±0.446	±0.128	±0.446
3+; av	±0.040	±0.201	±0.438	±0.120	±0.438
4+; $[SbF_6]^-$	±0.053	±0.245	±0.456	±0.149	±0.456

Vibrational and Electronic Absorption Spectra. Vibrational spectra of [HOC]^n (n = 0, 1+, 2+, 3+, 4+) are shown in Figure 5. There is a substantial shift in the frequency of the transition near 1500 cm^{-1} in HOC toward 1600 cm^{-1} as n increases. This band in HOC is tentatively assigned to a C_6-ring stretching mode.[27] The shift to higher frequency with increasing n is consistent with the assignment to stretching frequencies of the cyanine dye

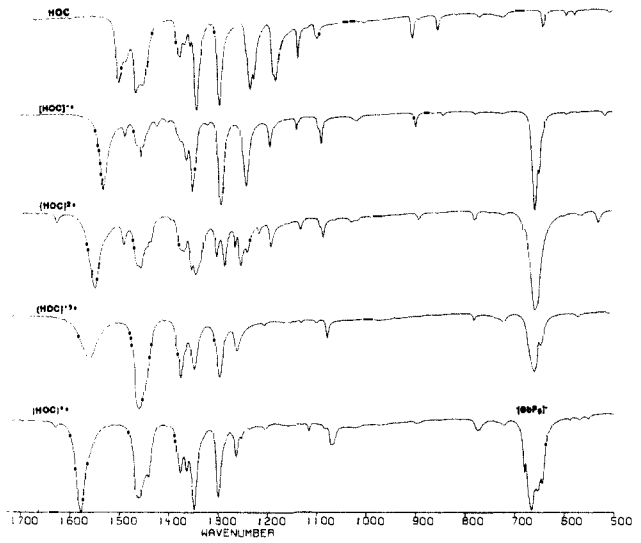

Figure 5. Infrared absorption spectra (Nujol) of $[HOC][SbF_6]_n$ (n = 0, 1+, 2+, 3+, 4+).

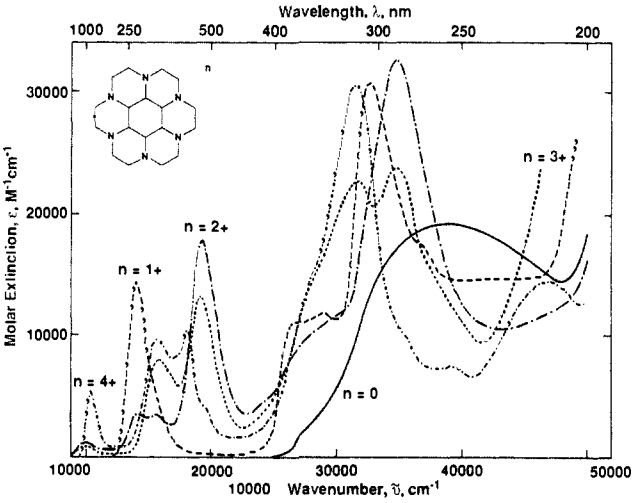

Figure 6. Electronic absorption spectra of HOC (CH_2Cl_2), $[HOC][BF_4]$, $[HOC][PF_6]_2$, $[HOC][PF_6]_3$, and $[HOC][SbF_6]_4$·MeCN (MeCN).

fragments. Calculations on a model cyanine dye **4a** show stretchings of the CN framework in this region.[28] Furthermore, calculations on $[CH_2{=}NH_2]^+$ also suggest a C=N stretch at 1620–1650 cm^{-1}.[28] A more detailed analysis of the vibrational spectra is not warranted at this time.

Due to the highly colored nature of the cationic species, only the Raman spectrum of HOC could be observed. The most intense band at 1608 cm^{-1} can be assigned to a degenerate C–C C_6-ring stretch and is essentially the same as the value of 1606 cm^{-1} found for liquid benzene.[27] The assignment of the other bands is not warranted at this time.

The UV–visible spectra of $[HOC]^n$ (n = 0–4) are shown in Figure 6 and are summarized in Table VI. For n = 0, the most significant transition near 38 000 cm^{-1} (260 nm) is the HOMO–LUMO transition and is very similar in energy to the absorption system near 260 nm in C_6H_6.[30] For n = 1+, there is an intense low-energy band in the region 14 000–15 000 cm^{-1}, a very intense band near 33 000 cm^{-1}, and two weaker bands near 29 000 and 26 600 cm^{-1}. The lowest energy absorption is tentatively assigned to a transition from the third highest occupied orbital to the singly occupied orbital (SOMO). The transition between the second highest occupied orbital and the SOMO is probably at too low an energy to be observed, since these orbitals were degenerate before the Jahn–Teller distortion occurred. The two weaker peaks at 26 600 and 28 900 cm^{-1} could be assigned to transitions from the fourth and fifth doubly occupied orbitals to the SOMO. These transitions are split by 2300 cm^{-1} (too large for a vibrational transition), and our admittedly crude calculation of this splitting is 1500 cm^{-1}. The very intense transition near 33 000 cm^{-1} is probably the SOMO–LUMO transition. We expect this transition in $[HOC]^{\cdot+}$ to be red-shifted from the comparable HOMO–LUMO transition in the neutral because removal of one electron should lead to an effective stabilization of the virtual orbitals. This transition is very similar in energy to that observed for the simple cyanine dye **4b**, which has its maximum absorption near 32 000 cm^{-1}.[31]

Table VI. Summary of Electronic Absorption Spectral Data for $[HOC]^n$ (n = 0,1+,2+,3+,4+)

	λ_{max},[f] nm	ν,[g] cm^{-1}	ϵ, cm^{-1} M^{-1} [h]
HOC[a]	260	38 450	17 900
$[HOC]^{\cdot+}$ [b]	303	33 000	23 400
	346	28 900	8 800
	376	26 600	8 400
	642 sh	15 575	4 050
	716	13 965	10 950
$[HOC]^{2+}$ [c]	292	34 250	26 950
	360 sh	27 780 sh	7 600
	524	19 080	17 200
	644	15 525	1 000
	710	14 080	1 050
	1000	9 900	1 100
$[HOC]^{\cdot 3+}$ [d]	290	34 500	20 175
	318	31 450	20 150
	366 sh	27 300 sh	10 200
	527	18 975	11 500
	636	15 725	7 000
	1000	10 000	1 500
$[HOC]^{4+}$ [e]	208	48 075	13 500
	260	38 450	6 875
	294 sh	34 100 sh	9 000
	323	30 950	29 100
	368 sh	27 175 sh	12 100
	510	19 600	4 025
	553	18 075	10 150
	640	15 625	9 375
	958	10 450	5 350

[a] HOC in CH_2Cl_2. [b] Average from $[HOC][PF_6]$, $[HOC][SbF_6]$, and $[HOC][BF_4]$ in MeCN. [c] Average from $[HOC][PF_6]_2$, $[HOC][SbF_6]_2$, $[HOC][AsF_6]_2$, $[HOC][SO_3CF_3]_2$, and $[HOC][BF_4]_2$ in MeCN. [d] Average from $[HOC][PF_6]_3$ and $[HOC][SbF_6]_3$ in MeCN. [e] $[HOC][SbF_6]_4$·MeCN in MeCN. [f] Absorption maxima. [g] Wavenumbers. [h] Molar extinction.

The spectrum for $[HOC]^{2+}$ exhibits a number of weak low-energy bands, an intense transition near 19 000 cm^{-1}, and a very intense transition near 34 000 cm^{-1}. The triplet is of comparable energy to the singlet (vide infra), complicating the spectral analysis. The low-intensity, low-energy transitions are probably due to excitations within the triplet manifold involving transitions from doubly occupied orbitals to the open shell orbitals. The 19 000-cm^{-1} absorption is also due to such occupied open shell transitions. The ~34 000-cm^{-1} absorption is assigned to an HOMO–LUMO transition of the singlet and is in the proper region for a transition involving uncoupled cyanine dyes.

The $[HOC]^{\cdot 3+}$ ion also exhibits a significant number of low-energy bands that are attributed to transitions from doubly occupied orbitals to the singly occupied degenerate pair of orbitals. One of the transitions near 30 000 cm^{-1} is again attributed to a HOMO–LUMO transition from the partially occupied e′ orbital to the unoccupied orbital derived from the LUMO of HOC.

A simple spectrum for $[HOC]^{4+}$ is expected for this closed shell singlet; however, a large number of spectral features are observed. As discussed previously, it was not obvious that $[HOC]^{4+}$ would be a closed shell singlet due to the mixing of the occupied orbitals of the benzene with the nitrogen lone pairs. It is apparent that, upon excitation, the orbitals reorder, leading to a complicated spectral pattern. The HOMO–LUMO (or cyanine dye) transition at 31 000 cm^{-1} is red-shifted from the analogous transitions in the other ions. There are a number of higher lying transitions that can be distinguished, including a feature near 48 000 cm^{-1}.

Magnetic Properties. Magnetic Susceptibility. The magnetic susceptibility of $[HOC]^n$ (n = 0, 1+, 2+, 3+, 4+) in the solid state

Table VII. Magnetic Susceptibility Parameters for $[HOC]^n$ (n = 0,1+,2+,3+,4+)

	χ_D,[a,c] 10^{-6} emu/mol	E_a,[b,d] kcal/mol	μ_{eff},[e] μ_B	θ,[f] K
HOC	−190			
$[HOC][BF_4]$	−240		1.76, 1.80	−2.0, −4.4
$[HOC][F_3CSO_3]$	−310		1.76	−3.4
[HOC][TCNE]	−250		2.48, 2.50	−49.7, 49.3
$[HOC]\{C[C(CN)_2]_3\}$	−352	3.7		
$[HOC][TCNQF_4]$	−130	3.7		
$[HOC]\{C_3[C(CN)_2]_3\}$	−259	see text		
$[HOC][C(CN)_3]_2$	−266	3.7		
$[HOC][BF_4]_2$	−228	3.4		
$[HOC][F_3CSO_3]_2$	−344	>4.0		
$[HOC][PF_6]_2$	−277	>4.0		
$[HOC][AsF_6]_2$	−334	>4.0		
$[HOC][SbF_6]_2$	−350	>4.0		
$[HOC]\{Ni[S_2C_2(CF_3)_2]_2\}_2$	−580		2.42, 2.44	−0.6, −1.2
$[HOC][TCNE]_2$	−304	3.7		
$[HOC][PF_6]_3$	−391		1.68, 1.74, 1.81	+0.2, −0.4, −1.3
$[HOC][SbF_6]_3$	−430		1.72, 1.79	−1.7, −1.9
$[HOC][SbF_6]_4$·MeCN	−570	>4.0		

[a] Diamagnetic corrections used: TCNE = 60 × 10^{-6} emu/mol; $[BF_4]^-$ = −32.2 × 10^{-6} emu/mol; $[PF_6]^-$ = −64.1 × 10^{-6} emu/mol; $[AsF_6]^-$ = −72 × 10^{-6} emu/mol; $[SbF_6]^-$ = −80 × 10^{-6} emu/mol; $Ni[S_2C_2(CF_3)_2]_2$ = −195.6 × 10^{-6} emu/mol; $[F_3CSO_3]^-$ = −77 × 10^{-6} emu/mol; $[C(CN)_3]^-$ = −38 × 10^{-6} emu/mol. $[i\text{-}C_4(CN)_6]^{2-}$ and $C_4(CN)_6$ = −162 × 10^{-6} emu/mol; $\{C_3[(CN)_2]_3\}^{2-}$ = −169 × 10^{-6} emu/mol. [b] ±0.4 kcal/mol. [c] Diamagnetic susceptibility. [d] Singlet-triplet separation. [e] Effective moment. [f] Curie–Weiss constant.

was determined by the Faraday method. The data demonstrate that the n = 0 and 4+ compounds are diamagnetic between 2.2 and 320 K, Table VII. HOC exhibits a diamagnetic susceptibility of −190 × 10^{-6} emu/mol at room temperature that agrees well with the value of −210 × 10^{-6} emu/mol calculated from the Pascal constants.[32] The magnetic susceptibilities of $[HOC]^n$ (n = 1+, 3+) obey the Curie–Weiss expression, $\chi = C/(T - \theta)$, between 2.2 and 320 K, Figure 7a. The average effective moment for these cations is 1.75 μ_B, consistent with the expectation of 1.73 μ_B for a doublet. The average Curie–Weiss constant θ of −2 K is typical for molecular materials and arises from dipolar interactions.

Crystalline salts of $[HOC]^{2+}$ with $[SbF_6]^-$, $[AsF_6]^-$, $[PF_6]^-$, and $[F_3CSO_3]^-$ counterions exhibit temperature-independent diamagnetic behavior below 320 K with small (≤0.5%) $S = {}^1/_2$ Curie contributions below 10 K (Figure 7b). The latter are attributed to $[HOC]^{\bullet+}$ impurities which are observed in the EPR spectra at <1% levels as simple absorptions at g = 2.0033 ($\Delta H \sim 30$ G). However, the EPR spectra of these salts in finely powdered form also show absorptions that are characteristic of randomly oriented triplets (vide infra). The intensity of these absorptions at room temperature is of the same order of magnitude as that of the radical impurities. Furthermore, it decreases rapidly with decreasing temperature, and the absorptions are not observed below ~100 K, indicating thermally populated triplet excited states. The EPR measurements (vide infra) show that the triplet excited state of $[HOC]^{2+}$ in its $[SbF_6]^-$, $[AsF_6]^-$, $[PF_6]^-$, and $[F_3CSO_3]^-$ salts is more than 4 kcal/mol above the ground singlet state. The temperature-dependent contribution of excited triplets to the magnetic susceptibility is given by the Bleaney–Bowers equation[35] (eq 1 where N is Avogadro's number, g is the Lande g factor, k_B

$$\chi = [g^2 N\mu_B{}^2/k_B T]/[3 + \exp(-\Delta E/k_B T)] \quad (1)$$

is the Boltzmann constant, μ_B is the Bohr magneton, and ΔE is the energy separation between the singlet ground state and the triplet excited state). However, the contribution to the susceptibility cannot be detected for this series of $[HOC]^{2+}$ salts since for $\Delta E > 4$ kcal/mol this contribution is below the sensitivity of the Faraday balance.

By contrast, the corrected molar susceptibilities of $[HOC][BF_4]_2$, $[HOC]^{2+}\{C[C(CN)_2]_3\}^{2-}$ (Figure 7b), $[HOC][C(CN)_3]_2$,

(35) Carlin, R. L. *Magnetochemistry*; Springer-Verlag: New York, 1986; p 75 ff.

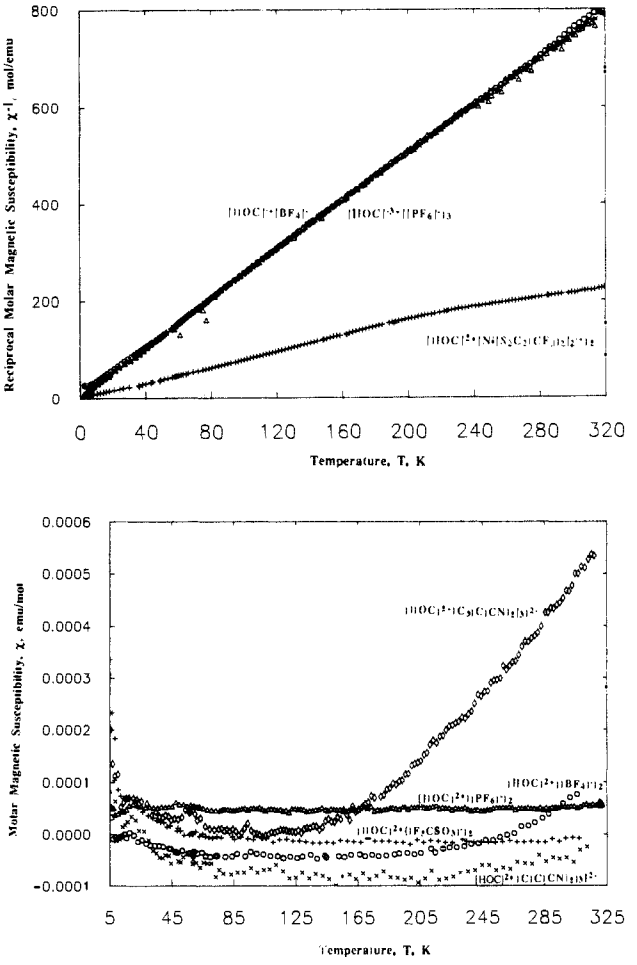

Figure 7. (a, top) Corrected reciprocal molar magnetic susceptibility, χ^{-1}, as a function of temperature for several $[HOC]^{\bullet+}[BF_4]^-$ (○), $[HOC]^{\cdot 3+}\{[PF_6]^-\}_3$ (△), and $[HOC]^{2+}\{[Ni[S_2C_2(CF_3)_2]_2]^-\}_2$ (+) salts. (b, bottom) Corrected molar magnetic susceptibility, χ, as a function of temperature for representative $[HOC]^{2+}$ salts: $\{[C[C(CN)_2]_3]^{2-}$ (×), $[BF_4]^-$ (○), $[PF_6]^-$ (△), $\{C_3[C(CN)_2]_3\}^{2-}$ (◇), and $[F_3CSO_3]^-$ (+)}. Essentially diamagnetic behavior is observed; however, the upturn at high temperatures results from a contribution of a thermally populated triplet (see text).

$[HOC]^{2+}[TCNQF_4]^{2-}$, and $[HOC]^{2+}[TCNE]_2{}^{2-}$ exhibit upturns at higher temperatures, indicating smaller singlet–triplet separations, ΔE. An estimate of ΔE can be obtained by least-squares fitting eq 1 to the higher temperature portions of the magnetic susceptibility curves. For $[HOC][BF_4]_2$, one obtains ΔE = 3.4 ± 0.4 kcal/mol (1710 K, 1190 cm^{-1}) in excellent agreement with 3.1 kcal/mol obtained by EPR measurements. For $[HOC][C(CN)_3]_2$, [HOC][TCNE]$_2$, and $[HOC]\{C[C(CN)_2]_3\}^{2-}$, slightly higher values of ΔE (3.7 ± 0.5 kcal/mol) were obtained, Table VII.

$[HOC]^{2+}\{C_3[C(CN)_2]_3\}^{2-}$ has a pronounced upturn in the magnetic susceptibility curve, Figure 7b. A similar least-squares fit to eq 1 yielded an energy of 2.1 kcal/mol. The latter, however, cannot be taken as the singlet–tripet gap for $[HOC]^{2+}$ since EPR measurements on the same material show, in addition to excited triplet $[HOC]^{2+}$, also the thermal population of an excited triplet species (and/or a species of higher spin multiplicity) with a much smaller D zero-field splitting parameter. This behavior is not understood and will be reexamined when an X-ray structural determination of this material becomes available.

The triplet excited state in $[HOC][TCNE]_2$ could be associated with either $[HOC]^{2+}$ or the $[TCNE]_2{}^{2-}$ dimer. Only the former applies, however, since a smaller D value would be expected for $[TCNE]_2{}^{2-}$. Thus, only the presence of excited $[HOC]^{2+}$ triplets is observed. This is further corroborated by the fact that neither $\{[Fe(C_5H_4)_2C_3H_6]^{\bullet+}\}_2[TCNE]_2{}^{2-}$,[26] $\{[Fe(C_5H_5)(C_5Me_5)]^{\bullet+}\}_2[TCNE]_2{}^{2-}$[TCNE]$^{\bullet 0}$THF,[29] nor $\{[Cr(C_6H_6)_2]^{\bullet+}\}_2[TCNE]_2{}^{2-}$,[36]

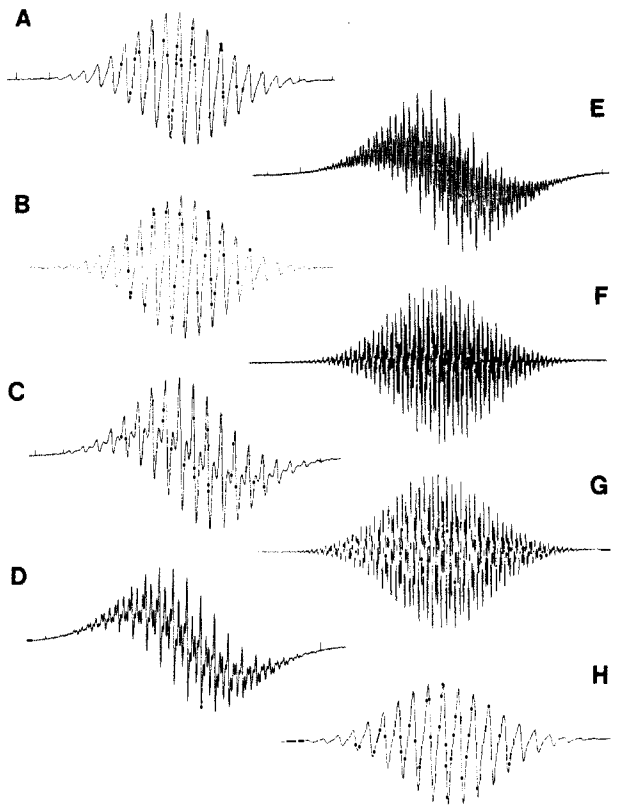

Figure 8. EPR spectra of $[HOC]^{\bullet+}[PF_6]^-$, in CH_2Cl_2 at 25 (A), −25 (C), −45 (D), −50 (E), and −90 °C (F). EPR spectrum of $[HOC]^{\bullet3+}\{[PF_6]^-\}_3$ at −45 °C in MeCN (H). Computer simulations of the EPR spectra of $[HOC]^{\bullet+}$ at 25 (B) and −90 °C (G).

which also possess $[TCNE]_2^{2-}$, exhibits evidence for a thermally populated triplet.[26,37]

The salts $[HOC]^{2+}\{Ni[S_2C_2(CF_3)_2]_2^{\bullet-}\}_2$ and $[HOC]^{\bullet+}[TCNE]^{\bullet-}$ have room-temperature effective moments of 2.46 ± 0.04 μ_B in agreement with the expectation of 2.45 μ_B for two independent spins. Thus, the susceptibility is attributed to the isolated radicals. The θ value for the former salt is −0.9 K and is consistent with essentially Curie–Weiss behavior. A deviation from Curie–Weiss behavior is evident at higher temperatures and is attributed to an increased susceptibility arising from thermally populated ^{3}-$[HOC]^{2+}$ contributing to the susceptibility. In contrast, the 1:1 $[HOC]^{\bullet+}[TCNE]^{\bullet-}$ salt exhibits substantial antiferromagnetic coupling, as evidenced by the large negative θ value of −49.6 K. The origin of the antiferromagnetic behavior is perplexing in view of the structure and is being investigated in greater detail.[38]

Electron Paramagnetic Resonance. $[HOC]^{\bullet+}$. The EPR spectrum of a dilute deep-blue CH_2Cl_2 solution of $[HOC]^{\bullet+}[PF_6]^-$ (1 mM, 25 °C) is shown in Figure 8A. The simplicity of this spectrum (g = 2.00315) indicates a large number of nuclei with approximately the same hyperfine splitting equal to the separation between adjacent lines. A computer simulation of this spectrum based on 6 equivalent nitrogens and 24 equivalent protons with splitting of 2.56 G (Figure 8B, ΔH = 0.7 G) matches the experimental spectrum. The observation of 24 equivalent protons suggests that the radical cation is highly flexible and that the two sets of 12 equatorial and 12 axial protons exchange very rapidly on the EPR time scale. Such an exchange can occur by synchronous inversions at two neighboring pyramidal N centers (see **12a**), causing a twist of the bond connecting two peripheral methylene groups. This twist converts an axial proton into an equatorial one and vice versa. Such inversions are unlikely to occur randomly without affecting the remaining N centers. More probably they are synchronously coupled.

As the temperature is lowered, the spectrum undergoes dramatic changes (Figure 8C–F), indicating that the exchange of the two sets of equivalent protons is slowing down. The slow-exchange limit is reached at around −90 °C (Figure 8F) as no changes occur upon further cooling. An ENDOR spectrum at approximately this temperature shows two pairs of absorptions centered around the free ^{1}H NMR frequency corresponding to two proton hyperfine couplings of 0.984 and 4.204 G. This information assured that two line spacings of 0.974 and 4.222 G, recurring throughout the complex EPR spectrum at −90 °C, are the hyperfine couplings of two sets of 12 equivalent protons, and that another recurring line spacing of 2.575 G is the coupling for six equivalent nitrogens. A computer simulation based on this assignment satisfactorily matches the experimental spectrum (ΔH = 0.23 G; Figure 8G).

The EPR spectrum of $[HOC]^{\bullet+}$ at −90 °C is consistent with a molecule with effective 6-fold symmetry precluding the observation of a dynamic Jahn–Teller distortion in solution by this technique. This is not surprising since all orbitally degenerate radicals studied by EPR so far (e.g., $[C_5H_5]^{\bullet}$,[39] benzene radical cation[40] and anion,[41] coronene radical cation[42] and anion,[43] etc.) also did not show such distortions in solution. Thus, it has been universally assumed that dynamic Jahn–Teller distorted structures interconvert in solution at rates that are fast on the EPR time scale.

The average of the hyperfine couplings for the axial and equatorial protons in the slow-exchange limit is 2.598 G if both couplings have the same sign. This average is very close to the coupling of the 24 equivalent protons at room temperature (2.56 G), confirming that the temperature dependence of the EPR spectra, Figure 8, is caused by line-shape effects that occur at intermediate rates of exchange, i.e., at rates comparable to the difference of the hyperfine couplings of the exchanging protons expressed in frequency units. Computer simulation of such temperature-dependent spectra can provide the rates for the exchange at given temperatures and hence the activation energy for the exchange from an Arrhenius plot. Unfortunately, existing computer programs for such calculations cannot handle two sets of 12 exchanging protons. An estimate of the rate of exchange, k, can nevertheless be made from the "coalescence" condition, eq 2,[44]

$$k = 2^{1/2}\pi\Delta a \qquad (2)$$

where Δa is the difference of the couplings of the exchanging protons expressed in cycles per second. We obtain $k = 4.04 \times 10^7$ s^{-1}. In our case, there is no obvious coalescence temperature, and we assume that coalescence occurs at a temperature midway between the fast- and slow-exchange limits, i.e., at 240 K. Assuming a form for the preexponential factor of $k_BT/h = 5 \times 10^{12}$ s^{-1} (where h is Planck's constant),[45] we obtain 5.6 kcal/mol as an estimate of the activation energy for the interconversion of equatorial and axial protons in $[HOC]^{\bullet+}$.

It has been pointed out above that the resonance structures for $[HOC]^{\bullet+}$ (Scheme II) are similar to those accepted for $[TMPD]^{\bullet+}$. $[HOC]^{\bullet+}$ can indeed be thought of as three fused TMPD structures (see Scheme II). The similarity is even more striking as $[TMPD]^{\bullet+}$, like $[HOC]^{\bullet+}$ in the fast-exchange limit, also has almost equal nitrogen and CH_3 proton couplings (6.99 and 6.76

(36) Lemervoskii, D. A.; Stukan, R. A.; Tarasevich, B. N.: Slovokhotov, Yu. L.; Antipin, M. Yu.; Kalinin, A. E.; Struchov, Yu. T. *Struct. Khim.* **1981**, *7*, 240.

(37) The $[TCNE]_2^{2-}$ dimers are separated by a short 2.9 Å. It is possible that such a dimer with a greater separation might have a smaller singlet–triplet energy gap and the triplet may be detectable by the Faraday method at 320 K.

(38) Laversanne, R.; Chackraborty, A.; Epstein, A. J.; Miller, J. S. In preparation.

(39) Liebling, G. R.; McConnell, H. M. *J. Chem. Phys.* **1965**, *42*, 3931.

(40) Carter, M. K.; Vincow, G. *J. Chem. Phys.* **1967**, *47*, 292.

(41) (a) Tuttle, T. R.; Weissman, S. I. *J. Am. Chem. Soc.* **1958**, *80*, 5342. (b) Fessenden, R. W.; Ogawa, S. *J. Am. Chem. Soc.* **1964**, *86*, 3591.

(42) Bolton, J. R.; Carrington, A. *Mol. Phys.* **1961**, *4*, 271.

(43) Townsend, M. G.; Weissman, S. I. *J. Chem. Phys.* **1960**, *32*, 309.

(44) Pople, J. A.; Schneider, W. G.; Bernstein, H. J. *High Resolution Nuclear Magnetic Resonance*; McGraw-Hill: New York, 1959; p 223.

(45) Levine, I. N. *Physical Chemistry*, 2nd ed.; McGraw-Hill: New York, 1983; p 805 ff. Wynne-jones, W. F. K.; Eyring, H. *J. Chem. Phys.* **1935**, *3*, 492.

Table VIII. Charge and Spin Distributions in $[HOC]^n$ (n = 0,+1,+2,+3,+4)

atom[a]	0	1+	2+ (1)	2+ (2)	2+ $[T(D_{3d})]^b$	2+ $[T(C_{2h})]^b$	3+[c]	4+
				Mulliken Charges, e				
C_1	0.06	0.13	0.19	0.10	0.13	0.13	0.19	0.19
C_2	0.06	0.04	0.02	0.22	0.13	0.13	0.10	0.19
N_1	−0.28	−0.26	−0.22	−0.26	−0.23	−0.23	−0.21	−0.17
N_2	−0.28	−0.26	−0.25	−0.18	−0.23	−0.23	−0.20	−0.17
C_H	0.11	0.18	0.21	0.21	0.22	0.22	0.28	0.37
				Spin Populations, e[d]				
C_1		0.29			0.10	0.08	−0.12	
C_2		−0.34			0.10	0.15	0.26	
N_1		0.14			0.26	0.28	0.08	
N_2		0.00			0.26	0.20	0.36	
S^2 (calc)		0.904			2.044	2.044	0.886	
S^2 (ideal)		0.75			2.0	2.0	0.75	

[a] See Table IV for atom labels. C_H refers to the CH_2 group charge. [b] Triplet states. [c] Calculated at experimental geometry. See text. [d] Calculated as α−β spins. There are always more α electrons. Positive implies excess α spin. Negative implies excess β spin.

Table IX. EPR Parameters for Triplets in $[HOC]^{2+}$ Salts[a]

	D, G	E, G	D, cm^{-1}	E, cm^{-1}	g_{xx}	g_{yy}	g_{zz}	ΔE, kcal/mol
$[HOC][SbF_6]_2$	597	20	0.0558	0.0019	2.0029	2.0027	2.0010	4.8
$[HOC][PF_6]_2$	595	23	0.0557	0.0022	2.0035	2.0034	2.0020	5.2
$[HOC][AsF_6]_2$	596	22	0.0558	0.0021	2.0029	2.0027	2.0018	5.9
$[HOC][BF_4]_2$	579	19	0.0542	0.0018	2.0018	2.0017	2.0010	3.1
$[HOC][BF_4]_2$[b]	596	22	0.0558	0.0021	2.0016	2.0014	2.0005	3.1
$[HOC][CF_3SO_3]_2$	581	26	0.0544	0.0024	2.0029	2.0028	2.0013	5.3
$[HOC][C(CN)_3]_2$	585	21	0.0547	0.0020	2.0033	2.0033	2.0011	3.4
$[HOC][C(CN)_3]_2$[c]	586	23	0.0548	0.0022	2.0044	2.0043	2.0021	3.4
$[HOC][TCNE]_2$	570	14	0.0533	0.0013				3.4
$[HOC]\{C[C(CN)_2]_3\}$	585	17	0.0547	0.0016				3.3

[a] 25 °C. [b] −50 °C. [c] Reference 33, single crystal.

G, respectively).[46] This is probably because the fast averaging of the equatorial and axial protons in $[HOC]^{\bullet+}$ is approximately equivalent, as concerns the β proton hyperfine interaction, to the averaging due to freely rotating methyl groups in $[TMPD]^{\bullet+}$. Using the description of three fused TMPD structures for HOC, we expect for $[HOC]^{\bullet+}$ couplings one-third of the values reported for $[TMPD]^{\bullet+}$, i.e., a^H = 2.33 G and a^N = 2.25 G, which are quite close to the 2.56 G measured for $[HOC]^{\bullet+}$.

The proton hyperfine couplings of freely rotating methyl groups attached to a radical center (β protons) have been used as an approximate measure of the π-spin density on carbon or nitrogen radical centers via

$$a_H^{Me} = Q_{CMe}\rho_C \quad \text{or} \quad a_H^{Me} = Q_{NMe}\rho_N$$

and a value of 42.9 G has been proposed for Q_{NMe} for alkylammonium radical cations.[47] Assuming again that the fast exchange of axial and equatorial methylene protons in $[HOC]^{\bullet+}$ is equivalent to a freely rotating β-CH_3 group, as the above comparison with $[TMPD]^{\bullet+}$ radical cation would suggest, we can estimate a spin density on nitrogen of 2.56/42.9 or 0.06. Although the approach is simplistic, this estimation is not far from the value obtained by ab initio calculations. By use of the data of Table VIII, the spin density on each nitrogen of $[HOC]^{\bullet+}$, rendered equivalent to all other N's by a rapid interconversion of the

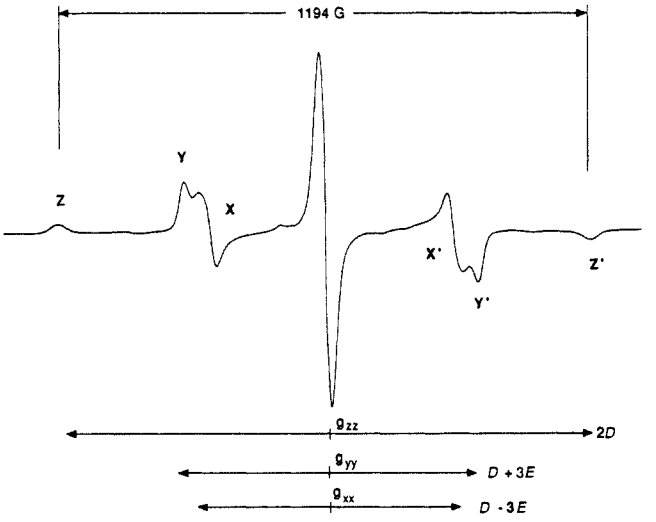

Figure 9. EPR spectrum of finely divided $[HOC][SbF_6]_2$ at 25 °C.

(46) Bolton, J. R.; Carrington, A.; dos Santos-Veiga, T. *J. Mol. Phys.* **1962**, *5*, 615.
(47) Danen, W. C.; Rickard, R. C. *J. Am. Chem. Soc.* **1972**, *94*, 3254.
(48) Richtsmeier, S. C.; Eades, R. A.; Dixon, D. A.; Gole, J. L. In *Metal Bonding and Interactions in High Temperature Systems*; Gole, J. L., Stwalley, W. C., Eds.; ACS Symposium Series 179; American Chemical Society: Washington, DC, 1982; p 177 and references therein. Mead, C. A. *J. Chem. Phys.* **1983**, *78*, 807; Thompson, T. C.; Truhlar, D. G.; Mead, C. A. *J. Chem. Phys.* **1985**, *82*, 2392; Truhlar, D. G.; Thompson, T. C.; Mead, C. A. *Chem. Phys. Lett.* **1986**, *127*, 287.
(49) Sutton, L. E. *Tables of Interatomic Distances and Configuration in Molecules and Ions*; Special Publication No. 11; The Chemical Society: London, 1958.
(50) Eades, R. A.; Weil, D. A.; Ellenberger, M. R.; Farneth, W. E.; Dixon, D. A.; Douglass, C. H., Jr. *J. Am. Chem. Soc.* **1981**, *103*, 5372. Kollman, P. A. *Adv. Org. Chem.* **1976**, *9*, 1.
(51) Armstrong, D. R.; Perkins, P. G.; Stewart, J. P. *J. Chem. Soc., Dalton Trans.* **1973**, 838.
(52) (a) Halgren, T. A.; Lipscomb, W. N. *Proc. Natl. Acad. Sci. U.S.A.* **1972**, *69*, 652. (b) Halgren, T. A.; Lipscomb, W. N. *J. Chem. Phys.* **1973**, *58*, 1569. (c) Marynick, D. S.; Lipscomb, W. N. *Proc. Natl. Acad. Sci. U.S.A.* **1982**, *79*, 1341.
(53) A stable triplet may not be necessary for an organic ferromagnet; two doublets with a virtually accessible triplet capable of admixing with the ground state, as observed for $[Fe^{III}(C_5Me_5)_2]^{\bullet+}[TCNE]^{\bullet-}$,[3,5] should suffice.
(54) Lapouyade, R.; Morand, J.-P. *J. Chem. Soc., Chem. Commun.* **1987**, 223.
(55) Wertz, J. E.; Bolton, J. R. *Electron Spin Resonance*; Chapman and Hall: London, 1972; p 244 and section 10-11.
(56) Suitable symmetrically trisubstituted benzenes might include, for example, S, O, and P atoms adjacent to the C_6 ring as well as replacement of C_6 atoms to form, for example, triazines, borazines, and cyclophosphazines.
(57) Jesse, R. E.; Biloen, P.; Prins, R.; van Voorst, J. D. W.; Hoijtink, G. *Mol. Phys.* **1963**, *6*, 633.

distorted structures, would be (4 × 0.14 + 2 × 0)/6 or 0.09 e.

[HOC]$^{2+}$. The EPR spectrum of a finely divided powder sample of [HOC][SbF_6]$_2$ at 25 °C has a g = 2.0033 central line (ΔH ~ 30 G) attributed to radical impurities at very low levels (<1%), most likely [HOC]$^{\bullet+}$ or [HOC]$^{\bullet 3+}$, Figure 9. The features to the left and right of this central line are absorptions characteristic of randomly oriented triplets[58] and can be analyzed in terms of the standard spin Hamiltonian[58,59] containing the electronic Zeeman term and the zero-field splitting term describing the dipolar interaction between two unpaired electrons in terms of two parameters, D and E, in the principal frame of reference. D provides a measure of the average distance between the interacting electrons in the triplet, while E is sensitive to the asymmetry of the triplet wave function and vanishes for wave functions with 3-fold and higher symmetry. A single-crystal study of [HOC][$C(CN)_3$]$_2$[33] has shown that the **g** and **D** tensors are parallel and that the direction of the largest component of the principal **D** tensor and the direction of the smallest component of the principal **g** tensor are within 1 deg of the normal to the central ring of the [HOC]$^{2+}$ cation (z axis). Since the **g** and **D** tensors are parallel, the five parameters of the spin Hamiltonian, g_{xx}, g_{yy}, g_{zz}, D, and E can be extracted by a nonlinear least-squares procedure from the analytical expressions[58,59] for the six resonance fields, labeled Z, Z', Y, Y', and X, X' in Figure 9, corresponding to the canonical orientations of the triplet in the magnetic field.

The EPR investigation shows that D and E are essentially invariant for several [HOC]$^{2+}$ salts and are in good agreement with the values obtained in the single-crystal study,[33] Table IX. The principal g values are determined less precisely due to the broad line width of the powder spectra and the uncertainty in locating the precise canonical axial fields.

The average distance between the two interacting electrons can be estimated[60] from D to be ~3.6 Å in [HOC]$^{2+}$, which is comparable to the dimensions of the π system. The nonvanishing asymmetry parameter E indicates a slight distortion of the excited triplet structure away from 3-fold symmetry. Ab initio calculations[33] of the D and E parameters for triplet [HOC]$^{2+}$ are consistent with a slight distortion toward the C_{2h} structure **1** of the singlet [HOC]$^{2+}$ host.

In addition to the $\Delta M = \pm 1$ triplet absorptions, the "forbidden" $\Delta M = \pm 2$ half-field absorption is also observed. The intensities of both absorptions decrease markedly with temperature, indicating that the triplet state in these crystalline materials is thermally populated and cannot be the ground state. The integrated intensities, measured at sufficiently low microwave powers to avoid saturation, of the $\Delta M = \pm 2$ absorption for [HOC][SbF_6]$_2$ at various temperatures can be fit by an equation analogous to the Bleaney–Bowers equation (eq 1) with a generalized least-squares procedure. This yields a 4.8 kcal/mol (1680 cm^{-1}; 2400 K; 210 meV) energy gap between the ground-state singlet and the excited triplet. The singlet–triplet energy separations were similarly determined for other [HOC]$^{2+}$ salts, Table IX. Good agreement between the powder and the single-crystal[33] ΔE's was obtained for [HOC][$C(CN)_3$]$_2$. All crystalline compounds in this study possess ^{3}[HOC]$^{2+}$ excited states at least 3.0 kcal/mol above the ground singlet state. The relationship of anion structure to ΔE will be discussed elsewhere together with the EPR results for frozen solutions of [HOC]$^{2+}$ salts.[34]

[HOC]$^{\bullet 3+}$. Since salts of this radical cation are insoluble in CH_2Cl_2 solution, EPR spectra were obtained using CH_3CN as the solvent. In striking contrast to the 1+ radical cation, the EPR spectrum of the 3+ radical cation is invariant as the temperature is lowered from 25 to −60 °C. (The latter could be reached by addition of a small amount of CH_2Cl_2.) The spectrum of a blood-red CH_3CN solution of [HOC]$^{\bullet 3+}$[PF_6^-]$_3$ at −45 °C is shown in Figure 8H. The spectrum appears to be identical to the 1+ radical cation at 25 °C. Careful measurements show, however, that both the g factor (2.003 10) and the separation between adjacent lines (2.81 G) are slightly different. Computer simulations of the spectrum confirm a hyperfine interaction of 2.81 G with 6 equivalent nitrogens and 24 equivalent protons. We conclude that the 3+ radical cation is undergoing exchange of equatorial and axial protons at faster rates than the 1+ analogue and that it exists in the fast-exchange limit even at −60 °C. This is consistent with the structural results (vide supra) which suggest that the trication would be more flexible than the monocation.

Molecular Orbital Calculations. HOC. The optimized structure for HOC has D_{3d} symmetry and is an energy minimum by analytic second derivative calculations. The bond distances are listed in the Table IV. The calculated C–C bond lengths in the benzene ring are in excellent agreement with the experimental values. The remaining calculated bond lengths are 0.03–0.04 Å too long. The charges are given in Table VIII. The benzenoid carbons are slightly positive (+0.06 e), and the nitrogens are quite negative (−0.28 e). The HOMO (4.6 eV) is degenerate (e_{1g} symmetry) and is essentially equally localized on the benzenoid carbons and on the nitrogens (see HOMO A and B). These results show that oxidation of HOC should lead to loss of electrons from both the nitrogen lone pairs as well as the benzene carbon π orbitals.

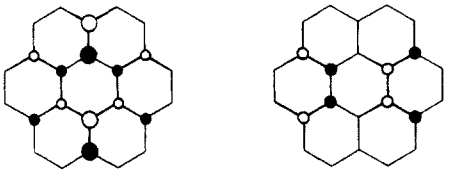

HOMO (A) HOMO (B)

[HOC]$^{\bullet+}$. As discussed previously, vertical removal of one electron from the HOMO of HOC leads to an $[\,]e^3$ occupancy and [HOC]$^{\bullet+}$ must undergo a Jahn–Teller distortion. Optimization of the structure of [HOC]$^{\bullet+}$ starting from either HOC or the two Jahn–Teller distorted structures for ^{1}[HOC]$^{2+}$, **1** and **2**, converged to the C_{2h} structure, **3**, in agreement with experimental observation. Comparison with the experimental structure for [HOC]$^{\bullet+}$[BF_4]$^-$ shows that the calculated C_6-ring C–C bond distances and the short C_6-ring C–N bond distances are 0.02 Å too long. The other C_6-ring C–N bond distance is 0.04 Å longer than calculated for HOC. The calculated C_H–N and C_H–C_H bond distances are also too long as compared to experiment.

Examination of the orbitals shows that the electron is removed from HOMO (B) and the electron occupancy is HOMO (A)^2 HOMO (B)^1. This set of orbital occupancies specifically influences the charge and spin distributions. The charge distribution shows that the four equivalent benzene carbons have lost 0.07 e each, but the two equivalent C_6-ring carbons have actually gained negative charge. This is consistent with the removal of an electron from HOMO (B) which has zero coefficients on the two equivalent carbon atoms and equal coefficients on the four equivalent carbons. Since HOMO (A) has excess density on the two equivalent carbons, it is not surprising that these two carbons gain in negative charge. The N's have become slightly more positive, and there is a loss of negative charge of 0.07 e on the CH_2 groups, showing an overall loss of negative charge in this region as expected from the orbital populations of HOC.

The spin population is defined as the difference in α and β spin populations. Since the electron is removed from HOMO (B), the largest positive spin population (excess α electrons) is on the four equivalent carbons. The amount of positive spin population on the four equivalent nitrogens is half the value on the carbons, Table VIII. The two equivalent nitrogens have no spin density consistent with the simplest orbital model. However, spin polarization of the benzene ring electrons leads to a large negative spin population on the two equivalent carbons. Since the orbital coefficients for the carbons and nitrogens are quite similar in the HOMO of HOC, the large spin polarization is consistent with the different magnitudes of the spins on the carbons and on the nitrogens. If the excess β spin population on the two equivalent carbons is divided among the four equivalent carbons and subtracted from the excess

(58) Wasserman, E.; Snyder, L. C.; Yeager, W. D. *J. Chem. Phys.* **1964**, *41*, 1763.
(59) Atherton, N. M. *Electron Spin Resonance*; Ellis Horwood: New York, 1973; Chapter 5.
(60) Abragam, A.; Bleaney, B. *Electron Paramagnetic Resonance of Transition Ions*; Clarendon Press: Oxford, 1970; p 508.

α spin population, the excess spin population on these carbons, 0.12 e, is comparable to that on the nitrogens.

$[HOC]^{2+}$. As discussed above, the electronic structure of the dication is formally derived from an e^2 orbital occupancy, leading to a ^3A or ^1E wave function, and the ^1E state undergoes a Jahn–Teller distortion. We first discuss the singlet states. The calculated structure of the singlet dication shows a significant deviation from the near 6-fold symmetry of the C_6N_6 moiety found in HOC. Starting from the crystal coordinates, a structure of approximate C_{2h} symmetry was optimized. This structure, **1**, has one negative direction of curvature at the Hartree–Fock level. Following this distortion, we reoptimized the structure, obtaining structure **2** with S_2 symmetry. Structure **2** is a true minimum on the Hartree–Fock surface and is 1.8 kcal/mol lower than structure **1** at the Hartree–Fock level. This situation reverses at the MP-2 correlated level, and structure **1** is 5.4 kcal/mol below **2**. Of course, the relative energies are only qualitative due to the small size of the basis set. The MP-2 corrections are qualitative but show the expected effect that the more delocalized structure is more highly correlated.

The agreement between the calculated geometry parameters for **1** and the experimental structure is very good. The calculated value for the C–C bond distance *a*, Table IV, is in excellent agreement with the experimental value. Distance *b* is consistent with a single C–C bond and is calculated to be 0.05 Å longer than observed and than expected for an sp^2–sp^2 C–C single bond.[49] The calculated C–N bond distance *c* in $[HOC]^{2+}$ is 0.1 Å shorter than calculated for HOC and is only 0.02 Å longer than the experimental value for $[HOC]^{2+}$. The remaining two C–N bond lengths, *d*, are calculated to lengthen slightly in $[HOC]^{2+}$ as compared to HOC. Thus, they remain as single C–N bonds. The calculated bond distances[28] for the model cyanine **4a** are r(C–C) = 1.389 Å and r(C–N) = 1.337 Å and are in excellent agreement with the calculated values for $[HOC]^{2+}$.

Structure **2** can also be described as one of the set of localized valence bond structures of the cyanine systems. The cyanine structures are localized with maximal unit charge separation. In contrast to structure **1**, there are two short C–C bonds, *b*, and C–N bonds, *d*, that have double bond lengths and four long C–C bonds, *a*, and C–N bonds, *c*, that are like single bonds. The four C–N bonds, *c*, are somewhat short as compared to the C–N bond lengths in the HOC.

The highest occupied molecular orbital and lowest unoccupied molecular orbital for $[HOC]^{2+}$ (**1** and **2**) are derived from the degenerate e_{1g} HOMO of HOC and are significantly split in energy. The HOMO of $[HOC]^{2+}$ **1** is HOMO (A) and the LUMO of HOC is HOMO (B), whereas for **2** this ordering is reversed. The HOMO for $[HOC]^{2+}$ **1** has at least as much nitrogen character as benzenoid carbon character as calculated for HOC. The shape of the HOMO is consistent with the distortion leading to the delocalized cyanine structures coupled by single bonds as discussed above. The largest density in the HOMO is found on the nitrogens not involved in the cyanine delocalization. The LUMO is antibonding between the C–N bonds in the cyanines.

The charge distributions for **1** and **2** are given in Table VIII. Since two electrons for **1** are removed from HOMO (B) of HOC, the positive charge on the four equivalent carbons should be significant as calculated and the two equivalent carbons actually gain negative charge as compared to HOC. The charges on the nitrogens follow the same trends. To form **2**, the electrons are removed from HOMO (A) of HOC and the charges are reversed. For **2**, the two equivalent carbons have more positive charge than do the four equivalent carbons. Furthermore the splitting of the nitrogen charges is increased.

The EPR results for $^3[HOC]^{2+}$ show structures with 3-fold, $E = 0$, and lower, $|E| \neq 0$, symmetries depending on the experimental conditions.[7,34] The geometry of the triplet was optimized with gradient techniques starting from two different structures: the D_{3d} symmetry structure of the HOC ground state and the C_{2h} symmetry structure, **1**, of singlet $[HOC]^{2+}$. Both structures converged toward a structure with D_{3d} symmetry. The calculated bond distances are given in Table IV for the D_{3d} structure. The calculated C_6-ring C–C bond length is 1.429 Å as compared to a value of 1.401 Å in HOC. The C_6-ring C–N bond length decreases from 1.453 Å in HOC to 1.383 Å in $[HOC]^{2+}$. Based on the HOC orbitals, more electron density would be lost from the N lone pairs than from the benzene, leading to more iminium character (and shortening) in the C_6-ring C–N bonds. A distorted C_{2h} structure that is 0.9 kcal/mol higher in energy than the D_{3d} structure was obtained from the optimization path beginning from the singlet C_{2h} geometry. The distorted structure has four short 1.375-Å distances and two long 1.390-Å distances. Calculations of *D* and *E* for this distorted structure are consistent with the experimental results.[33]

Analysis of the wave functions for the D_{3d} and C_{2h} triplet structures shows a striking difference in the electronic structures considering the small differences in energy and geometry, Table VIII. The atomic charges for the triplets are the average of those for the distorted singlets. The spin populations of the D_{3d}-like structure are symmetric with spin populations of 0.102 e on the C_6-ring carbons and of 0.255 e on the nitrogen; there is clearly more excess spin density on N than on the C_6-ring carbon, in clear contrast to the spin-polarized results calculated for $[HOC]^{\bullet+}$. The spin populations in the C_{2h} structure are clearly asymmetric. There are four C_6-ring carbons with spin populations of 0.080 e and four N's associated with these carbons with spin populations of 0.280 e. The other two C_6-ring carbons have increased their spin population to 0.152 e and the N's associated with these carbons have spin populations decreased to 0.204 e. Note that the spin population associated with each C–N bonding region is constant for the D_{3d} and C_{2h} structures. The change from D_{3d} in spin populations on the nitrogens in the C_{2h} structure is like that found for $[HOC]^{\bullet+}$, whereas the corresponding change for the carbons is opposite to that found for $[HOC]^{\bullet+}$. The change in spin populations on the carbons is like that found for $[HOC]^{\bullet 3+}$ (vide infra). The distorted triplet incorporates a component from the $[HOC]^{\bullet+}$ structure for the nitrogens that is balanced by a component from the $[HOC]^{\bullet 3+}$ structure for the carbons.

$[HOC]^{\bullet 3+}$. Three electrons are removed from the degenerate HOMO of HOC to form the $n = 3+$ species. The single remaining electron occupies either HOMO (A) or HOMO (B). The similarity in energy of these two states, the excess positive charge, and lower lying π orbitals of the same symmetry complicate the calculations. Initial geometry optimization led to a structure with low symmetry and an unacceptable S^2 value [$S^2 = S(S + 1)$]. Geometry optimization was further complicated by poor convergence in the SCF and subsequent loss of symmetry combined with unacceptably high values of S^2. However, we were able to obtain a partially optimized structure whose bond distances are given in Table IV. The C_6-ring C–C bonds are too long when compared to experiment, but the calculated difference between the length of bonds *a* and *b* (0.015 Å) is similar to the experimentally observed difference of 0.022 Å. The calculated C_6-ring C–N bonds show a larger difference than observed experimentally. In conformity with the results for the previous species, both the N–CH_2 and CH_2–CH_2 bond lengths are calculated to be longer than the experimental values.

Because of the complications noted above, we employed the $[HOC]^{\bullet 3+}$ experimental geometry derived from the crystal structure for $[HOC][PF_6]_3$ (with idealized values for r(C–H) of 1.08 Å and θ(HCH) of 109°) for the charge and spin calculations, Table VIII. The charges clearly show more excess positive charge on the four equivalent carbons compared to the other two carbons. This follows from the orbital occupancies where both electrons from HOMO (B) of HOC and one electron from HOMO (A) have been removed. Although the nitrogens have negative charge, the CH_2 group charges have increased in positive character, showing the large positive charge in the external portions of the molecule. The excess spin populations are also consistent with our simple orbital model. Since the single electron is in HOMO (A), the largest spin population should indeed be on the two equivalent carbons and nitrogens. The largest excess α spin population is found on the two nitrogens followed by the two

carbons. There is also excess α spin population (0.08 e) on the four equivalent nitrogens. In contrast, there is excess β spin population on the four equivalent carbons, showing a large spin polarization in the C_6 ring as calculated for $[HOC]^{\bullet+}$. If the excess β spins in the benzene ring are subtracted from the excess α spins in this ring, the net excess α spin population in the ring is only 0.02 e, showing that most of the excess spin is on the nitrogens.

As noted above, the EPR results indicated rapid exchange of the equatorial and axial protons for the $n = 1+$ and $3+$ cations. The low energy for interconversion of the Jahn–Teller distorted structures for these doublet states parallels the low barriers for interchanging different symmetry structures found in the M_3 systems where M is a group IA or IB metal.[48] The M_3 systems have three equivalent $^2A_1$ (acute angle) and three equivalent $^2B_2$ (obtuse angle) structures which are the two types of C_{2v} distortions from the D_{3h} structure. The $[HOC]^{\bullet+}$ and $[HOC]^{\bullet 3+}$ doublets have similar manifolds of structures with three equivalent coupled cyanine dye structures and three equivalent *p*-phenylenediiminium structures for the C_{2h} distortions from the D_{3d} structure. Extensive studies on these Jahn–Teller distorting M_3 doublets show that asymmetric vibrations interconvert the various $^2A_1$ and $^2B_2$ states without ever accessing the ^2E state in D_{3h} symmetry. The ^2E state sits at the conical intersection of the potential surfaces and is much higher in energy. Similar motions with very low barriers would also be expected in $[HOC]^{\bullet+}$ and $[HOC]^{\bullet 3+}$ especially since the changes in geometry are not large, in agreement with the observed EPR results. A second motion is responsible for the interconversion of the axial and equatorial protons on the CH_2 groups. This motion is a normal conformational change as discussed above involving an effective concerted inversion at N. The data show that for $[HOC]^{\bullet+}$ this conformational motion can be separated from the motion about the conical intersection. Since this conformational motion can be resolved in the $[HOC]^{\bullet+}$ system, it gives an upper limit of ~5.6 kcal/mol for the barriers for motion about the conical intersection. The actual barriers for the motion about the conical intersection are clearly much lower than this upper limit. The increased flexibility of the $[HOC]^{\bullet 3+}$ structure did not allow us to separate these two motions in our EPR study.

$[HOC]^{4+}$. The geometry of $[HOC]^{4+}$ was gradient optimized as a singlet and is a minimum as shown by analytic second derivative calculations. The calculated bond distances are presented in Table IV. The calculated C_6-ring C–C bond distance in $[HOC]^{4+}$ is 0.04 Å longer than the average experimental value. The other calculated bond distances in $[HOC]^{4+}$ are 0.012–0.034 Å longer than the experimental values and show the identical trends found in the calculations for HOC and $[HOC]^{2+}$. (The expanded calculated external C_H–C_H and C_H–N bond distances allow the calculated internal C_6-ring C–C and C–N bond distances to be longer.) The calculations parallel the experimentally observed increase in nonplanarity of the C_6N_6 moiety in going from HOC to $[HOC]^{4+}$.

The calculated charge distribution for $[HOC]^{4+}$ (Table VIII) shows C_6-ring carbons with a charge of 0.19 e and nitrogens with a charge of −0.17 e. The group charges for the CH_2 groups are 0.37 e. These can be compared to the charges in HOC of 0.06 e on C_6-ring carbons, −0.28 e on N, and 0.11 e on the CH_2 groups. Clearly the largest change in the charge distribution is on the external portion of the molecule. The charge removed from C_6-ring carbons and nitrogens is approximately equal. Most of the excess charge was on the CH_2 groups rather than the nitrogen region or the benzene regions. This is consistent with the modest lengthening of the C_6-ring C–C bond distances and with the dramatic decrease in the C_6-ring C–N distance which is approaching the C–N bond distance found in protonated imines [r(C–N) = 1.29 Å].[50] As expected from our calculations on HOC, the HOMO for $[HOC]^{4+}$ is nondegenerate and is predominantly an out-of-plane p orbital on C_6-ring carbons and nitrogen; the LUMO is a degenerate pair of orbitals. Consistent with the charge distributions, the coefficients for the $[HOC]^{4+}$ LUMO are larger on the nitrogen than on the C_6-ring carbons.

Bond Order. A quantitative definition of the total bond order has been given by Armstrong et al.[51] in terms of the degree of bonding. The bond orders were calculated with wave functions determined by the PRDDO method, which explicitly includes all electrons in a minimum basis set of Slater orbitals.[52] The same exponents employed in the STO-3G calculations were employed. Calculations were only carried out for structures with D_{3d} symmetry [$n = 0$, $n = 2+$ (triplet), and $n = 4+$] at the optimized geometries (vide supra). The calculated total bond orders and bond lengths are given in Table IV. For comparison, the calculated C–C bond order for benzene at the experimental bond distance of 1.397 Å is 1.44, whereas a valence bond definition yields a value of 1.5. For HOC, we find a slightly smaller C–C bond order of 1.37. The C–N bond order in HOC is slightly above the value of 1.00 expected for a single bond. For $^3[HOC]^{2+}$, there is a significant decrease in the C–C bond order and an increase in the C–N bond order so that both values are nearly identical. These trends continue in $[HOC]^{4+}$ with a C–C bond order more like that of a single bond and a C–N bond order higher than the C–C bond order in benzene.

Implications for the Design of Stable Organic Triplet Species. The McConnell mechanism[1-3] for the stabilization of localized ferromagnetic coupling in a molecular solid requires the configurational mixing of a ground state possessing a doubly degenerate orbital with a low-lying charge-transfer excited state with spin conservation. Thus, stable radicals ($S \geq {}^1/_2$) are a necessary component in the design of a molecular/organic ferromagnet.[2,3,53] If the isolated species was a ground-state singlet with a small singlet–triplet energy separation, electrostatic and charge-transfer interactions could stabilize the triplet and lead to ferromagnetic behavior. However, the crystalline salts of $[HOC]^{2+}$ reported here are ground-state singlets and thus would be inappropriate for this purpose. The original motivation for studying $[HOC]^n$ was to synthesize an organic/molecular ferromagnet based on the 1:1 electron-transfer complex between TCNE and HOC. Since $[HOC]^{\bullet+}[TCNE]^{\bullet-}$ exhibits strong antiferromagnetic, not ferromagnetic, behavior, this objective was not realized.

The results for $[HOC]^{2+}$ suggested that significant care must be taken in order to design organic triplet-based molecular ferromagnets. Other hexaaza-substituted benzene dications, such as the dication of 2,3:6,7:10,11-tris(*N*,*N*′-diethylenediammino)-triphenylene,[4,9] or hexamethoxytriphenylene,[4] may also have singlet ground states, and their structures and magnetic properties should be investigated at low temperature. The compounds tris(ethylenedithio)benzene, tris[(ethyleneoxy)thio]benzene, and tris(methylenedithio)benzene, have been prepared as a model for an organic ferromagnet;[54] however, their dications also may be singlets, and a determination of their spin multiplicity would be of interest.

Stabilization of the triplet ground state, thus, requires a lack of dominance by singlet resonance structures; hence, materials with a negative value for the electron exchange integral for the diradical electrons should be sought.[55] A triplet compatible with the hexachlorobenzene dication was observed under conditions expected to lead to its formation.[10] Elimination of pseudo-6-fold symmetry may destabilize the Jahn–Teller distorted singlet ground state, enabling the formation of the triplet. For example, the dication of the triaza-substituted benzene **13**,[56] although it may form a singlet resonance structure, **13a**, could have a triplet ground state, **13b**, because both formal plus charges are on the iminium nitrogens leading to better charge separation.

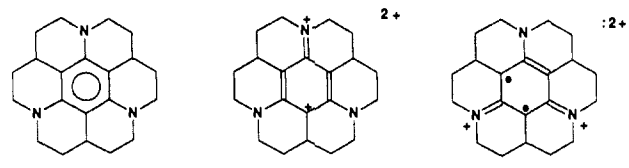

13 **13a** **13b**

Triplet dianion species should also be investigated with the goal of preparing stable organic triplets as components for s/p-orbital-based molecular ferromagnets. The dianions of decacyclene and 1,3,5-triphenylbenzene have been reported to have triplet ground states, though the coronene dianion is a singlet with a

thermally accessible triplet.[57] Sufficiently strong donors that stabilize these dianions and could form the desired $\cdots D^{2+}A^{\cdot 2-}D^{2+}A^{\cdot 2-}D^{2+}A^{\cdot 2-}\cdots$ structure are unknown. Hexacyanotriphenylene, **14**, or dodecacyanodecacyclene, **15**, dianions, however, might be suitable compounds to prepare as a component for an s/p-orbital-based ferromagnet.

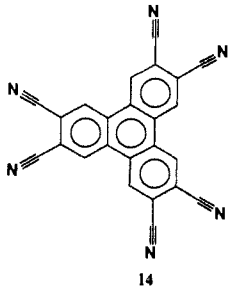

14

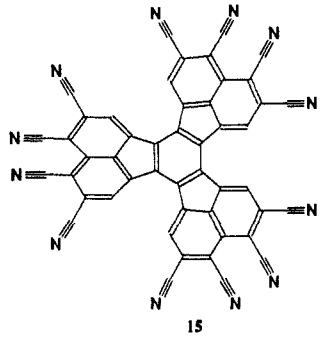

15

Stable organic triplet ground-state species are of fundamental scientific interest and the possibility that they might be a viable components for s/p-orbital-based molecular ferromagnet enhances their scientific/technological value. Dications and dianions of six-membered-ring systems with 3-fold symmetry designed to frustrate the singlet ground state should be investigated.

Acknowledgment. We express our appreciation to the colleagues who helped us in several experimental areas: D. Wipf in synthesis, W. Marshall in X-ray diffraction, R. S. McLean in magnetic susceptibility, S. Hill and W. Barney in EPR, D. B. Chase in Raman and IR spectroscopies, F. Davidson and D. Ovenall in NMR, and E. Matthews and R. Richardson in electronic and vibrational spectroscopies. Thanks are due also to Prof. H. van Willigen (University of Massachusetts, Boston) for having taken several ENDOR spectra, to Prof. R. Breslow (Columbia University) for kindly providing a preprint prior to publication, and to K. Preston and J. R. Morton (NRC, Ottawa) for many insightful discussions.

Registry No. HOC, 92187-27-4; $[HOC]^{\cdot+}[BPh_4]^-$, 114491-13-3; $[HOC]^{\cdot+}[BF_4]$, 123265-28-1; $[HOC]^{\bullet+}[PF_6]^-$, 123265-12-3; $[HOC]^{\cdot+}[SbF_6]^-$, 114530-89-1; $[HOC]^{\bullet+}[AsF_6]^-$, 123265-13-4; $[HOC]^{\cdot+}[F_3CSO_3]^-$, 123265-14-5; $[HOC]^{\bullet+}[TCNE]^{\bullet-}$, 123265-15-6; $[HOC]^{\cdot+}[TCNQ]^{\bullet-}$, 123265-16-7; $[HOC]^{2+}[n\text{-}C_4(CN)_6]^{2-}$, 123265-17-8; $[HOC]^{\cdot+}[DDQ]^{\bullet-}$, 123265-18-9; $[HOC]^{2+}[TCNQF_4]^{2-}$, 123265-19-0; $[HOC]^{2+}\{C_3[C(CN)_2]_3\}^{2-}$, 123265-20-3; $[HOC]^{2+}\{[TCNE]^{\bullet-}\}_2$, 123265-21-4; $[HOC]^{2+}\{[FB_4]^-\}_2$, 117346-46-0; $[HOC]^{2+}\{[PF_3]^-\}_2$, 117346-47-1; $[HOC]^{2+}\{[AsF_6]^-\}_2$, 123265-22-5; $[HOC]^{2+}\{[F_3CSO_3]^-\}_2$, 123265-23-6; $[HOC]^{2+}\{[SbF_6]^-\}_2$, 123265-25-8; $[HOC]^{2+}\{Ni[S_2C_2(CF_3)_2]_2^{\bullet-}\}_2$, 123265-26-9; $[HOC]^{2+}\{[C(CN)_3]^-\}_2$, 121919-38-8; $[HOC]^{2+}\{C_3[C(CN)_2]_3^{\cdot-}\}_2$, 123289-02-1; $[HOC]^{2+}\{C[C(CN)_2]_3\}^{2-}$, 123289-01-0; $[HOC]^{\cdot 3+}\{[PF_6]^-\}_3$, 123265-24-7; $[HOC]^{\bullet 3+}\{[SbF_6]^-\}_3$, 123265-27-0; $[HOC]^{4+}\{[SbF_6]^-\}_4\cdot MeCN$, 118399-45-4; $[HOC]^{\bullet+}$, 92187-28-5; $[HOC]^{2+}$, 92187-29-6; $[HOC]^{3+}$, 92187-30-9; $[HOC]^{4+}$, 92187-31-0; 2a,4a,6a,8a,10a,12a-hexaazacoronene-1,3,5,7,9,11(2*H*,4*H*,6*H*,8*H*,10*H*,12*H*)-hexone, 92187-33-2.

Supplementary Material Available: Figures showing stereoviews and anion labeling and tables listing anion bond distances and angles, fractional coordinates/anisotropic thermal parameters, intermolecular separations, electronic absorption maxima and their extinction coefficients, and deviations from least-squares planes for HOC, $[HOC][BF_4]$, $[HOC][F_3CSO_3]$, [HOC][TCNE], $[HOC][BF_4]_2$, $[HOC][PF_6]_2$, $[HOC]\{Ni[S_2C_2(CF_3)_2]_2\}_2$, $[HOC][C(CN)_3]_2$, $[HOC]\{C[C(CN)_2]_3\}$, $[HOC][PF_6]_3$, $[HOC][SbF_6]_3$, and $[HOC][SbF_6]_4\cdot MeCN$, as well as optimized structures for $[HOC]^n$ (n = 0, 1+, 2+, 3+, 4+) (119 pages); tables of calculated and observed structure factors (58 pages). Ordering information is given on any current masthead page.

Photochemistry of Diphenylketyl Radicals in Polar Solvents[1]

R. W. Redmond, J. C. Scaiano,* and L. J. Johnston*

Contribution from the Division of Chemistry, National Research Council, Ottawa, Canada K1A 0R6. *Received May 18, 1989*

Abstract: The photolysis of diphenylketyl radicals in acetonitrile leads to their photobleaching with a quantum yield of 0.10. The decay of the excited radicals occurs by four different pathways: (a) doublet–doublet fluorescence; (b) radiationless decay; (c) electron photoejection, which accounts for 20% of the observed bleaching; and (d) O–H bond cleavage leading to benzophenone, which is presumed to account for the remaining 80% of the bleaching. The electrons produced in acetonitrile are trapped by ground-state benzophenone to yield its radical anion (λ_{max} 710 nm); addition of electron scavengers (N_2O or acetone) prevents the formation of $Ph_2CO^{\bullet-}$.

The photochemistry and photophysics of a number of radicals have recently attracted considerable attention.[2-11] For example, the fluorescence lifetimes and quenching behavior of a variety of arylmethyl-type radicals have been examined. The majority of these radicals do not undergo any net photochemistry from their excited states, although quenching of the excited states with various substrates may often lead to different products from those formed from the ground-state radical. In contrast, several ketyl radicals do yield products upon excitation.[12-15] The diphenylketyl radical

(1) Issued as NRCC 30765.
(2) Scaiano, J. C.; Johnston, L. J.; McGimpsey, W. G.; Weir, D. *Acc. Chem. Res.* **1988**, *21*, 22-29.
(3) Scaiano, J. C.; Johnston, L. J. *Pure Appl. Chem.* **1986**, *58*, 1273-1278.
(4) Scaiano, J. C.; Johnston, L. J. *Org. Photochem.* **1989**, *10*.
(5) Scaiano, J. C.; Tanner, M.; Weir, D. *J. Am. Chem. Soc.* **1985**, *107*, 4396-4403.
(6) Bromberg, A.; Schmidt, K. H.; Meisel, D. *J. Am. Chem. Soc.* **1985**, *107*, 83-91.
(7) Johnston, L. J.; Scaiano, J. C. *J. Am. Chem. Soc.* **1985**, *107*, 6368-6372.
(8) Hilinski, E. F.; Huppert, D.; Kelley, D. F.; Milton, S. V.; Rentzepis, P. M. *J. Am. Chem. Soc.* **1984**, *106*, 1951-1957.
(9) Tokumura, K.; Mizukami, N.; Udagawa, M.; Itoh, M. *J. Phys. Chem.* **1986**, *90*, 3873-3876.
(10) Weir, D.; Johnston, L. J.; Scaiano, J. C. *J. Phys. Chem.* **1988**, *92*, 1742-1746.
(11) Meisel, D.; Das, P. K.; Hug, G. L.; Bhattacharyya, K.; Fessenden, R. W. *J. Am. Chem. Soc.* **1986**, *108*, 4706-4710.
(12) Johnston, L. J.; Lougnot, D. J.; Wintgens, V.; Scaiano, J. C. *J. Am. Chem. Soc.* **1988**, *110*, 518-524.
(13) Johnston, L. J.; Lougnot, D. J.; Scaiano, J. C. *Chem. Phys. Lett.* **1986**, *129*, 205-210.

0002-7863/90/1512-398$02.50/0 Published 1990 by the American Chemical Society